



20 November 2017

Dear Dr. Peylin,

My co-authors and I are pleased to submit our revised manuscript titled “*Impacts of microtopographic snow-redistribution and lateral subsurface processes on hydrologic and thermal states in an Arctic polygonal ground ecosystem*” for your consideration for publication in *Geoscientific Model Development*.

We thank you for your constructive feedbacks, which helped us to clarify important aspects of our work. Modifications made in the revised version of the manuscript are summarized below:

1. We have added text in Section 2.6 (lines 309 – 311) to acknowledge that the location of sensors does not align with 2D transect used for modeling.
2. Our work shows that explicitly resolving snow redistribution due to microtopography and lateral subsurface processes does not have an impact on domain average hydrologic and thermal states. Thus, we believe additional studies are needed to justify the need to explicitly account for fine-scale processes. Possible future extensions of our work include representing intermediate scale topographical variation and biogeochemical cycles along with snow redistribution and lateral subsurface processes in the model. We have expanded Section 3.5 (lines 533 – 537) to recommend this type of extension of our work.
3. We have updated Figure 1 to clarify the extent of the study site.
4. Captions of Figure 4 and 6 have been updated.
5. Two missing references on Page 2 Line 56 of second submission have been added.
6. The sentence in Section 3.5 has been corrected.
7. Additionally, the U.S. Department of Energy has renamed the Accelerated Climate Modeling for Energy (ACME) to the [Energy Exascale Earth System Model](#) (E3SM). Thus, all reference to ACME and ACME Land Model (ALM) have been changed to E3SM and E3SM Land Model (ELM) in the revised manuscript.

My co-authors and I believe we have thoroughly addressed your comments and that the revised manuscript is well suited for publication in *Geoscientific Model Development*. We look forward to receiving your response.

Sincerely,  
Gautam Bisht

1 **Impacts of microtopographic snow-redistribution and lateral subsurface processes**  
2 **on hydrologic and thermal states in an Arctic polygonal ground ecosystem : A case**  
3 **study using [ELM-3D v1.0](#)**

4  
5 **Gautam Bisht<sup>1</sup>, William J. Riley<sup>1</sup>, Haruko M. Wainwright<sup>1</sup>, Baptiste Dafflon<sup>1</sup>, Yuan**  
6 **Fengming<sup>2</sup>, and Vladimir E. Romanovsky<sup>3</sup>**

7  
8 <sup>1</sup>Climate & Ecosystem Sciences Division, Lawrence Berkeley National Laboratory,1  
9 Cyclotron Road, Berkeley, California 94720, USA

10  
11 <sup>2</sup>Environmental Sciences Division, Oak Ridge National Laboratory, Oak Ridge, TN, 37831-  
12 6301 , USA

13  
14 <sup>3</sup>Geophysical Institute, University of Alaska Fairbanks, Fairbanks, AK 99775, USA

15  
16 Correspondence to: Gautam Bisht (gbisht@lbl.gov)

17  
18 **Abstract**

19 Microtopographic features, such as polygonal ground, are characteristic sources of  
20 landscape heterogeneity in the Alaskan Arctic coastal plain. Here, we analyze the effects of  
21 snow redistribution (SR) and lateral subsurface processes on hydrologic and thermal states  
22 at a polygonal tundra site near Barrow, Alaska. We extended the land model integrated in  
23 the [E3SM](#) to redistribute incoming snow by accounting for microtopography and  
24 incorporated subsurface lateral transport of water and energy ([ELM-3D v1.0](#)). Multiple 10-  
25 years long simulations were performed for a transect across polygonal tundra landscape at  
26 the Barrow Environmental Observatory in Alaska to isolate the impact of SR and  
27 subsurface process representation. When SR was included, model predictions better  
28 agreed (higher R<sup>2</sup>, lower bias and RMSE) with observed differences in snow depth between  
29 polygonal rims and centers. The model was also able to accurately reproduce observed soil  
30 temperature vertical profiles in the polygon rims and centers (overall bias, RMSE, and R<sup>2</sup> of  
31 0.59°C, 1.82°C, and 0.99, respectively). The spatial heterogeneity of snow depth during the

Gautam Bisht 11/14/2017 1:02 PM  
Deleted: ALM

Gautam Bisht 11/14/2017 1:02 PM  
Deleted: ACME Earth System Model (ESM)

Gautam Bisht 11/14/2017 1:02 PM  
Deleted: ALM

35 winter due to SR generated surface soil temperature heterogeneity that propagated in  
36 depth and time and led to ~10 cm shallower and ~5 cm deeper maximum annual thaw  
37 depths under the polygon rims and centers, respectively. Additionally, SR led to spatial  
38 heterogeneity in surface energy fluxes and soil moisture during the summer. Excluding  
39 lateral subsurface hydrologic and thermal processes led to small effects on mean states but  
40 an overestimation of spatial variability in soil moisture and soil temperature as subsurface  
41 liquid pressure and thermal gradients were artificially prevented from spatially dissipating  
42 over time. The effect of lateral subsurface processes on maximum thaw depths was modest,  
43 with mean absolute differences of ~3 cm. Our integration of three-dimensional subsurface  
44 hydrologic and thermal subsurface dynamics in the [E3SM](#) land model will facilitate a wide  
45 range of analyses heretofore impossible in an ESM context.

Gautam Bisht 11/14/2017 1:02 PM

Deleted: ACME

## 46 1 Introduction

47 The northern circumpolar permafrost region, which contains ~1700 Pg of organic  
48 carbon down to 3 m (Tarnocai et al., 2009), is predicted to experience disproportionately  
49 larger future warming compared to the tropics and temperate latitudes (Holland and Bitz,  
50 2003). Recent warming in the Arctic has led to changes in lake area (Smith et al., 2005),  
51 snow cover duration and extent (Callaghan et al., 2011a), vegetation cover (Sturm et al.,  
52 2005), growing season length (Smith et al., 2004), thaw depth (Schuur et al., 2008),  
53 permafrost stability (Jorgenson et al., 2006), and land-atmosphere feedbacks (Euskirchen  
54 et al., 2009). Future predictions of Arctic warming include northward expansion of shrub  
55 cover in tundra ([Sturm et al., 2001](#); [Tape et al., 2006](#)), decreases in snow cover duration  
56 (Callaghan et al., 2011a), and emissions of CO<sub>2</sub> and CH<sub>4</sub> from decomposition of  
57 belowground soil organic matter (Koven et al., 2011; Schaefer et al., 2011; Schuur and  
58 Abbott, 2011; Xu et al., 2016).

Gautam Bisht 11/14/2017 1:02 PM

Deleted: (strum 2001, Tape et al 2006),

59 Several recent modeling studies have predicted a positive global carbon-climate  
60 feedback at the global scale (Cox et al., 2000; Dufresne et al., 2002; Friedlingstein et al.,  
61 2001; Fung et al., 2005; Govindasamy et al., 2011; Jiang et al., 2011; Jones et al., 2003;  
62 Koven et al., 2015; Matthews et al., [2007a](#); Matthews et al., 2005; Sitch et al., 2008;  
63 Thompson et al., 2004; Zeng et al., 2004), although the strength of this predicted feedback

Gautam Bisht 11/14/2017 1:02 PM

Deleted: 2007b

67 at the year 2100 was shown to have a large variability across models (Friedlingstein et al.,  
68 2006). In contrast to the ocean carbon cycle, the terrestrial carbon cycle is expected to be a  
69 more dominant factor in the global carbon-climate feedback over the next century  
70 (Matthews et al., 2007b; Randerson et al., 2015).

71 Snow, which covers the Arctic ecosystem for 8-10 months each year (Callaghan et  
72 al., 2011b), is a critical factor influencing hydrologic and ecologic interactions (Jones,  
73 1999). Snowpack modifies surface energy balances (via high reflectivity), soil thermal  
74 regimes (due to low thermal conductivity), and hydrologic cycles (because of melt water).  
75 Several studies have shown that warm soil temperatures under snowpack support the  
76 emission of greenhouse gases from belowground respiration (Grogan and Chapin III, 1999;  
77 Sullivan, 2010) and nitrogen mineralization (Borner et al., 2008; Schimel et al., 2004)  
78 during winter. Additionally, decreases in snow cover duration have been shown to increase  
79 net ecosystem CO<sub>2</sub> uptake (Galen and Stanton, 1995; Groendahl et al., 2007). Recent snow  
80 manipulation experiments in the Arctic have provided evidence of the importance of snow  
81 in the expected responses of Arctic ecosystems under future climate change (Morgner et al.,  
82 2010; Nobrega and Grogan, 2007; Rogers et al., 2011; Schimel et al., 2004; Wahren et al.,  
83 2005; Welker et al., 2000).

84 Apart from the spatial extent and duration of snowpack, the spatial heterogeneity of  
85 snow depth is an important factor in various terrestrial processes (Clark et al., 2011;  
86 Lundquist and Dettinger, 2005). As synthesized by López-Moreno et al. (2014), the  
87 following processes are responsible for snow depth heterogeneity at three distinct spatial  
88 scales: microtopography at 1-10 m (Lopez-Moreno et al., 2011); wind induced lateral  
89 transport processes at 100-1000 m (Liston et al., 2007); and precipitation variability at  
90 catchment scales of 10 – 1000 km (Sexstone and Fassnacht, 2014). The spatial distribution  
91 of snow not only affects the quantity of snowmelt discharge (Hartman et al., 1999; Luce et  
92 al., 1998), but also the water chemistry (Rohrbough et al., 2003; Wadham et al., 2006;  
93 Williams et al., 2001). Lawrence and Swenson (2011) demonstrated the importance of  
94 snow depth heterogeneity in predicting responses of the Arctic ecosystem to future climate  
95 change by performing idealized numerical simulations of shrub expansion across the pan-  
96 Arctic region using the Community Land Model (CLM4). Their results showed that an  
97 increase in active layer thickness (ALT), which is the maximum annual thaw depth, under

Gautam Bisht 11/14/2017 1:02 PM

Deleted: 2007a



99 shrubs was negated when spatial heterogeneity in snow cover due to wind driven snow  
100 redistribution was accounted for, resulting in an unchanged grid cell mean active layer  
101 thickness.

102 Large portions of the Arctic are characterized by polygonal ground features, which  
103 are formed in permafrost soil when frozen ground cracks due to thermal contraction  
104 during winter and ice wedges form within the upper several meters (Hinkel et al., 2005).  
105 Polygons can be classified as ‘low-centered’ or ‘high-centered’ based on the relationship  
106 between their central and mean elevations. Polygonal ground features are dynamic  
107 components of the Arctic landscape in which the upper part of ice-wedge thaw under low-  
108 centered polygon troughs leads to subsidence, eventually (~o(centuries)) converting the  
109 low-centered polygon into a high-centered polygon (Seppala et al., 1991). Microtopography  
110 of polygonal ground influences soil hydrologic and thermal conditions (Engstrom et al.,  
111 2005). In addition to controlling CO<sub>2</sub> and CH<sub>4</sub> emissions, soil moisture affects (1)  
112 partitioning of incoming radiation into latent, sensible, and ground heat fluxes (Hinzman  
113 and Kane, 1992; McFadden et al., 1998); (2) photosynthesis rates (McGuire et al., 2000;  
114 Oberbauer et al., 1991; Oechel et al., 1993; Zona et al., 2011); and (3) vegetation  
115 distributions (Wiggins, 1951).

116 Our goals in this study include (1) analyzing the effects of spatially heterogeneous  
117 snow in polygonal ground on soil temperature and moisture and surface processes (e.g.,  
118 surface energy budgets); (2) analyzing how model predictions are affected by inclusion of  
119 lateral subsurface hydrologic and thermal processes; and (3) developing and testing a  
120 three-dimensional version of the ~~E3SM~~ Land Model (~~ELM~~; (Tang and Riley, 2016; Zhu and  
121 Riley, 2015)), called ~~ELM~~-3D v1.0 (hereafter ~~ELM~~-3D). We then applied ~~ELM~~-3D to a  
122 transect across a polygonal tundra landscape at the Barrow Environmental Observatory in  
123 Alaska. After defining our study site, the model improvements, model tests against  
124 observations, and analyses, we apply the model to examine the effects of snow  
125 redistribution and lateral subsurface processes on snow micro-topographical  
126 heterogeneity, soil temperature, and the surface energy budget.

Gautam Bisht 11/14/2017 1:02 PM

Deleted: ACME

Gautam Bisht 11/14/2017 1:02 PM

Deleted: ALM

Gautam Bisht 11/14/2017 1:02 PM

Deleted: ALM

Gautam Bisht 11/14/2017 1:02 PM

Deleted: ALM

Gautam Bisht 11/14/2017 1:02 PM

Deleted: ALM

132 **2 Methodology**

133 **2.1 Study Area**

134 Our analysis focuses on sites located near Barrow, Alaska (71.3° N, 156.5° W) from  
135 the long term Department of Energy (DOE) Next-Generation Ecosystem Experiment (NGEE-  
136 Arctic) project. The four primary NGEE-Arctic study sites (A, B, C, D) are located within the  
137 Barrow Environmental Observatory (BEO), which is situated on the Alaskan Coastal Plain.  
138 The annual mean air temperature for our study sites is approximately -13°C (Walker et al.,  
139 2005) and mean annual precipitation is 106 mm with the majority of precipitation  
140 occurring during the summer season (Wu et al., 2013). The study site is underlain with  
141 continuous permafrost (Brown et al., 1980) and the annual maximum thaw depth (active  
142 layer depth) ranges between 30-90 cm (Hinkel et al., 2003). Although the overall  
143 topographic relief for the BEO is low, the four NGEE study sites have distinct  
144 microtopographic features: low-centered (A), high-centered (B), and transitional polygons  
145 (C, D). Contrasting polygon types are indicative of different stages of permafrost  
146 degradation and were the primary motivation behind the choice of study sites for the  
147 NGEE-Arctic project. LIDAR Digital Elevation Model (DEM) data were available at 0.25 m  
148 resolution for the region encompassing all four NGEE sites. In this work, we perform  
149 simulations along a two-dimensional transect in low-centered polygon Site-A as shown by  
150 the dotted line in [Figure 1](#),

151 **2.2 ~~ELM~~v0 Description**

152 The original version of [ELM](#) is equivalent to CLM4.5 ([Ghimire et al., 2016](#); Koven et  
153 al., 2013; Oleson, [2013a](#)), and represents vertical energy and water dynamics, including  
154 phase change. We developed [ELM](#)-3D by expanding on that model to explicitly represent  
155 soil lateral energy and hydrological exchanges and fine-resolution snow redistribution. We  
156 run [ELM](#)-3D here with prescribed plant phenology (called Satellite Phenology (SP) mode),  
157 since our focus is on thermal dynamics of the system, rather than C cycle dynamics.

Gautam Bisht 11/14/2017 1:03 PM  
Deleted: Figure 1

Gautam Bisht 11/14/2017 1:02 PM  
Deleted: ALMv0

Gautam Bisht 11/14/2017 1:02 PM  
Deleted: ALM

Gautam Bisht 11/14/2017 1:02 PM  
Deleted: 2013b; Ghimire et al., 2016

Gautam Bisht 11/14/2017 1:02 PM  
Deleted: ALM

Gautam Bisht 11/14/2017 1:02 PM  
Deleted: ALM

## 164 2.3 Representing Two- and Three-Dimensional Physics

### 165 2.3.1 Subsurface hydrology

166 The flow of water in the unsaturated zone is given by the  $\theta$ -based Richards  
167 equations as

$$\frac{\partial \theta}{\partial t} = -\nabla \cdot \vec{q} - Q \quad (1)$$

168 where  $\theta$  [ $\text{m}^3\text{m}^{-3}$ ] is the volumetric soil water content,  $t$  [s] is time,  $\vec{q}$  [ $\text{ms}^{-1}$ ] is Darcy flux, and  
169  $Q$  [ $\text{m}^{-3}$  of water  $\text{m}^{-3}$  of soil  $\text{s}^{-1}$ ] is volumetric sink of water. Darcy flux is given by

$$\vec{q} = -k\nabla(\psi + z) \quad (2)$$

170 where  $k$  [ $\text{ms}^{-1}$ ] is the hydraulic conductivity,  $\psi$  [m] is the soil matric potential, and  $z$  [m] is  
171 height above a reference datum. The hydraulic conductivity and soil matric potential are  
172 non-linear functions of volumetric soil moisture. [ELMv0](#) uses the modified form of Richards  
173 equation of Zeng and Decker (2009) that computes Darcy flux as

$$\vec{q} = -k\nabla(\psi + z - C) \quad (3)$$

174 where  $C$  is a constant hydraulic potential above the water table,  $z_v$ , given as

$$C = \psi_E + z = \psi_{sat} \left[ \frac{\theta_E(z)}{\theta_{sat}} \right]^{-B} + z = \psi_{sat} + z_v \quad (4)$$

175 where  $\psi_E$  [m] is the equilibrium soil matric potential,  $\psi_{sat}$  [m] is the saturated soil matric  
176 potential,  $\theta_E$  [ $\text{m}^3\text{m}^{-3}$ ] is volumetric soil water content at equilibrium soil matric potential,  
177  $\theta_{sat}$  [ $\text{m}^3\text{m}^{-3}$ ] is volumetric soil water content at saturation,  $z_v$  [m] is height of water table  
178 above the reference datum, and  $B$  [-] is a fitting parameter for soil-water characteristic  
179 curves. Substituting equations (3) and (4) into equation (1) yields the equation for the  
180 vertical transport of water in [ELMv0](#):

$$\frac{\partial \theta}{\partial t} = \frac{\partial}{\partial z} \left[ k \left( \frac{\partial(\psi - \psi_E)}{\partial z} \right) \right] - Q \quad (5)$$

181 A finite volume spatial discretization and implicit temporal discretization with Taylor  
182 series expansion leads to a tri-diagonal system of equations. We extended this 1-D Richards  
183 equation to a 3-D representation integrated in [ELM-3D](#), which is presented next.

184 We use a cell-centered finite volume discretization to decompose the spatial domain  
185 into  $N$  non-overlapping control volumes,  $\Omega_n$ , such that  $\Omega = \cup_{n=1}^N \Omega_n$  and  $\Gamma_n$  represents the

Gautam Bisht 11/14/2017 1:02 PM

Deleted: ALMv0

Gautam Bisht 11/14/2017 1:02 PM

Deleted: ALMv0

Gautam Bisht 11/14/2017 1:02 PM

Deleted: ALM

189 boundary of the  $n$ -th control volume. Applying a finite volume integral to equation (1) and  
 190 the divergence theorem yields

$$\frac{\partial}{\partial t} \int_{\Omega_n} \theta dV = - \int_{\Gamma_n} (\vec{q} \cdot d\vec{A}) - \int_{\Omega_n} Q dV \quad (6)$$

191 The spatially discretized equation for the  $n$ -th grid cell that has  $V_n$  volume and  $n'$  neighbors  
 192 is given by

$$\frac{d\theta_n}{dt} V_n = - \sum_{n'} (\vec{q}_{nn'} \cdot \vec{A}_{nn'}) - Q V_n \quad (7)$$

193 For the sake of simplicity in presenting the discretized equation, we assume the 3-D grid is  
 194 a Cartesian grid with each grid cell having a thickness of  $\Delta x$ ,  $\Delta y$ , and  $\Delta z$  in the  $x$ ,  $y$ , and  $z$   
 195 directions, respectively. Using an implicit time integral, the 3-D discretized equation at time  
 196  $t + 1$  for a  $(i, j, k)$  control volume is given as

$$\begin{aligned} \left( \frac{\Delta \theta_{i,j,k}^{t+1}}{\Delta t} \right) V_{i,j,k} &= \left( q_{x_{i-1/2,j,k}}^{t+1} - q_{x_{i+1/2,j,k}}^{t+1} \right) \Delta y \Delta z \\ &+ \left( q_{y_{i,j-1/2,k}}^{t+1} - q_{y_{i,j+1/2,k}}^{t+1} \right) \Delta x \Delta z \\ &+ \left( q_{z_{i,j,k-1/2}}^{t+1} - q_{z_{i,j,k+1/2}}^{t+1} \right) \Delta x \Delta y - Q V_{i,j,k} \end{aligned} \quad (8)$$

197 where  $q_x$ ,  $q_y$  and  $q_z$  are Darcy flux in the  $x$ ,  $y$ , and  $z$  directions, respectively and  $\Delta \theta_{i,j,k}^{t+1}$  is the  
 198 change in volumetric soil liquid water in time  $\Delta t$ . [Using the same approach as Oleson](#)  
 199 [\(2013b\), the Darcy flux in all three directions is linearized about  \$\theta\$  using Taylor series](#)  
 200 [expansion](#). The linearized Darcy flux in the  $x$  direction at the  $(i - 1/2, j, k)$  interface is a  
 201 function of  $\theta_{i-1,j,k}$  and  $\theta_{i,j,k}$ :

$$q_{x_{i-1/2,j,k}}^{t+1} = q_{x_{i-1/2,j,k}}^t + \frac{\partial q_{x_{i-1/2,j,k}}^t}{\partial \theta_{i-1,j,k}} \Delta \theta_{i-1,j,k}^{t+1} + \frac{\partial q_{x_{i-1/2,j,k}}^t}{\partial \theta_{i,j,k}} \Delta \theta_{i,j,k}^{t+1} \quad (9)$$

202 The linearized Darcy fluxes in the  $y$  and  $z$  directions are computed similarly. Substituting  
 203 equation (9) in equation (8) results in a banded matrix of the form

$$\begin{aligned} \alpha \Delta \theta_{i-1,j,k}^{t+1} + \beta \Delta \theta_{i,j-1,k}^{t+1} + \gamma \Delta \theta_{i,j,k-1}^{t+1} + \eta \Delta \theta_{i+1,j,k}^{t+1} + \mu \Delta \theta_{i,j+1,k}^{t+1} + \phi \Delta \theta_{i,j,k+1}^{t+1} \\ + \zeta \Delta \theta_{i,j,k}^{t+1} = \varphi \end{aligned} \quad (10)$$

204 where  $\alpha$ ,  $\beta$ , and  $\gamma$  are subdiagonal entries;  $\eta$ ,  $\mu$ , and  $\phi$  are superdiagonal entries;  $\zeta$  is  
 205 diagonal entry of the banded matrix is given by

Gautam Bisht 11/14/2017 1:02 PM  
**Deleted:** Using the same approach as Oleson (2013a), the Darcy flux in all three directions is linearized about  $\theta$  using Taylor series expansion.

$$\alpha = \frac{\partial q_{x_{i-1/2,j,k}}^t}{\partial \theta_{i-1,j,k}} \Delta y \Delta z \quad (11)$$

$$\beta = \frac{\partial q_{y_{i,j-1/2,k}}^t}{\partial \theta_{i,j-1,k}} \Delta x \Delta z \quad (12)$$

$$\gamma = \frac{\partial q_{z_{i,j,k-1/2}}^t}{\partial \theta_{i,j,k-1}} \Delta x \Delta y \quad (13)$$

$$\eta = \frac{\partial q_{x_{i+1/2,j,k}}^t}{\partial \theta_{i+1,j,k}} \Delta y \Delta z \quad (14)$$

$$\mu = \frac{\partial q_{y_{i,j+1/2,k}}^t}{\partial \theta_{i,j+1,k}} \Delta x \Delta z \quad (15)$$

$$\phi = \frac{\partial q_{z_{i,j,k+1/2}}^t}{\partial \theta_{i,j,k+1}} \Delta x \Delta y \quad (16)$$

$$\begin{aligned} \zeta = & \left( \frac{\partial q_{x_{i-1/2,j,k}}^t}{\partial \theta_{i,j,k}} - \frac{\partial q_{x_{i+1/2,j,k}}^t}{\partial \theta_{i,j,k}} \right) \Delta y \Delta z + \left( \frac{\partial q_{y_{i,j-1/2,k}}^t}{\partial \theta_{i,j,k}} - \frac{\partial q_{y_{i,j+1/2,k}}^t}{\partial \theta_{i,j,k}} \right) \Delta x \Delta z \\ & + \left( \frac{\partial q_{z_{i,j,k-1/2}}^t}{\partial \theta_{i,j,k}} - \frac{\partial q_{z_{i,j,k+1/2}}^t}{\partial \theta_{i,j,k}} \right) \Delta x \Delta y - \frac{\Delta x \Delta y \Delta z}{\Delta t} \end{aligned} \quad (17)$$

210

211 The column vector  $\varphi$  is given by

$$\begin{aligned} \varphi = & - \left( q_{x_{i-1/2,j,k}}^t - q_{x_{i+1/2,j,k}}^t \right) \Delta y \Delta z - \left( q_{y_{i,j-1/2,k}}^t - q_{y_{i,j+1/2,k}}^t \right) \Delta x \Delta z \\ & - \left( q_{z_{i,j,k-1/2}}^t - q_{z_{i,j,k+1/2}}^t \right) \Delta x \Delta y + Q_{i,j,k}^{t+1} \Delta x \Delta y \Delta z \end{aligned} \quad (18)$$

212

213 The coefficients of equation (10) described in equation (11)-(18) are for an internal grid  
 214 cell with six neighbors. The coefficients for the top and bottom grid cells are modified for  
 215 infiltration and interaction with the unconfined aquifer in the same manner as [Oleson](#)  
 216 [\(2013b\)](#). Similarly, the coefficients for the grid cells on the lateral boundary are modified  
 217 for a no-flux boundary condition. See [Oleson \(2013b\)](#) for details about the computation of  
 218 hydraulic properties and derivative of Darcy flux with respect to soil liquid water content.

Gautam Bisht 11/14/2017 1:02 PM  
 Deleted: Oleson (2013a).

Unknown  
 Field Code Changed

Gautam Bisht 11/14/2017 1:02 PM  
 Deleted: 2013a

### 2.3.2 Subsurface thermal

[ELMv0](#) solves a tightly coupled system of equations for soil, snow, and standing water temperature ([Oleson, 2013a](#)). The model solves the transient conservation of energy:

$$c \frac{\partial T}{\partial t} = -\nabla \cdot \mathbf{F} \quad (19)$$

where  $c$  is the volumetric heat capacity [ $\text{J m}^{-3} \text{K}^{-1}$ ],  $\mathbf{F}$  is the heat flux [ $\text{W m}^{-2}$ ], and  $t$  is time [s]. The heat conduction flux is given by

$$\mathbf{F} = -\lambda \nabla T \quad (20)$$

where  $\lambda$  is thermal conductivity [ $\text{W m}^{-1} \text{K}^{-1}$ ] and  $T$  is temperature [K]. Applying a finite volume integral to equation (20) and divergence theorem yields

$$c \frac{\partial}{\partial t} \int_{\Omega_n} T = - \int_{\Gamma_n} \vec{\mathbf{F}} \cdot d\vec{\mathbf{A}} \quad (21)$$

The spatially discretized equation for a  $n$ -th grid cell that has  $V_n$  volume and  $n'$  neighbors is given by

$$c_n \frac{dT_n}{dt} V_n = - \sum_{n'} (\vec{\mathbf{F}}_{nn'} \cdot \vec{\mathbf{A}}_{nn'}) \quad (22)$$

Similar to the approach taken in Section 2.3.1, [ELM-3D](#) assumes a 3-D Cartesian grid with each grid cell having a thickness of  $\Delta x$ ,  $\Delta y$ , and  $\Delta z$  in the  $x$ ,  $y$ , and  $z$  directions, respectively. Temporal integration of equation (22) is carried out using the Crank-Nicholson method that uses a linear combination of fluxes evaluated at time  $t$  and  $t + 1$ :

$$\begin{aligned} c_{n_{i,j,k}} \frac{(T_{i,j,k}^{t+1} - T_{i,j,k}^t)}{\Delta t} \Delta x \Delta y \Delta z \\ = \omega \left\{ \left( F_{x_{i-\frac{1}{2},j,k}}^t - F_{x_{i+\frac{1}{2},j,k}}^t \right) \Delta y \Delta z + \left( F_{y_{i,j-\frac{1}{2},k}}^t - F_{y_{i,j+\frac{1}{2},k}}^t \right) \Delta x \Delta z \right. \\ \left. + \left( F_{z_{i,j,k-\frac{1}{2}}}^t - F_{z_{i,j,k+\frac{1}{2}}}^t \right) \Delta x \Delta y \right\} \\ + (1 - \omega) \left\{ \left( F_{x_{i-\frac{1}{2},j,k}}^{t+1} - F_{x_{i+\frac{1}{2},j,k}}^{t+1} \right) \Delta y \Delta z \right. \\ \left. + \left( F_{y_{i,j-\frac{1}{2},k}}^{t+1} - F_{y_{i,j+\frac{1}{2},k}}^{t+1} \right) \Delta x \Delta z \right. \\ \left. + \left( F_{z_{i,j,k-\frac{1}{2}}}^{t+1} - F_{z_{i,j,k+\frac{1}{2}}}^t + 1 \right) \Delta x \Delta y \right\} \end{aligned} \quad (23)$$

Gautam Bisht 11/14/2017 1:02 PM

Deleted: ALMv0

Gautam Bisht 11/14/2017 1:02 PM

Deleted: (Oleson, 2013b).

Gautam Bisht 11/14/2017 1:02 PM

Deleted: ALM

237 where  $\omega$  is the weight in the Crank-Nicholson method and set to 0.5 in this study.

238 Substituting a discretized form of heat flux using equation (20) in equation (23), results in  
 239 a banded matrix of the form

$$\alpha T_{i-1,j,k}^{t+1} + \beta T_{i,j-1,k}^{t+1} + \gamma T_{i,j,k-1}^{t+1} + \eta T_{i+1,j,k}^{t+1} + \mu T_{i,j+1,k}^{t+1} + \phi T_{i,j,k+1}^{t+1} + \zeta \Delta T_{i,j,k}^{t+1} = \varphi \quad (24)$$

240 where  $\alpha, \beta$ , and  $\gamma$  are subdiagonal entries;  $\eta, \mu$ , and  $\phi$  are superdiagonal entries;  $\zeta$  is  
 241 diagonal entry of the banded matrix is given by

$$\alpha = \left( \frac{-(1-\omega)\Delta t}{c_{n_{i,j,k}}\Delta x} \right) \left( \frac{\lambda_{i-1/2,j,k}}{x_{i,j,k} - x_{i-1,j,k}} \right) \quad (25)$$

242

$$\beta = \left( \frac{-(1-\omega)\Delta t}{c_{n_{i,j,k}}\Delta y} \right) \left( \frac{\lambda_{i,j-1/2,k}}{y_{i,j,k} - y_{i-1,j,k}} \right) \quad (26)$$

243

$$\gamma = \left( \frac{-(1-\omega)\Delta t}{c_{n_{i,j,k}}\Delta z} \right) \left( \frac{\lambda_{i,j,k-1/2}}{z_{i,j,k} - z_{i,j,k-1}} \right) \quad (27)$$

244

$$\eta = \left( \frac{-(1-\omega)\Delta t}{c_{n_{i,j,k}}\Delta x} \right) \left( \frac{\lambda_{i+1/2,j,k}}{x_{i+1,j,k} - x_{i,j,k}} \right) \quad (28)$$

245

$$\mu = \left( \frac{-(1-\omega)\Delta t}{c_{n_{i,j,k}}\Delta y} \right) \left( \frac{\lambda_{i-1/2,j,k}}{y_{i+1,j,k} - y_{i,j,k}} \right) \quad (29)$$

246

$$\phi = \left( \frac{-(1-\omega)\Delta t}{c_{n_{i,j,k}}\Delta z} \right) \left( \frac{\lambda_{i-1/2,j,k}}{z_{i+1,j,k} - z_{i,j,k}} \right) \quad (30)$$

247

$$\begin{aligned} \zeta = 1 + & \left( \frac{(1-\omega)\Delta t}{c_{n_{i,j,k}}\Delta x} \right) \left[ \frac{\lambda_{i-1/2,j,k}}{x_{i,j,k} - x_{i-1,j,k}} + \frac{\lambda_{i+1/2,j,k}}{x_{i+1,j,k} - x_{i,j,k}} \right] \\ & + \left( \frac{(1-\omega)\Delta t}{c_{n_{i,j,k}}\Delta y} \right) \left[ \frac{\lambda_{i,j-1/2,k}}{y_{i,j,k} - y_{i,j-1,k}} + \frac{\lambda_{i,j+1/2,k}}{y_{i,j+1,k} - y_{i,j,k}} \right] \\ & + \left( \frac{(1-\omega)\Delta t}{c_{n_{i,j,k}}\Delta z} \right) \left[ \frac{\lambda_{i,j,k-1/2}}{z_{i,j,k} - z_{i,j,k-1}} + \frac{\lambda_{i,j,k+1/2}}{z_{i,j,k+1} - z_{i,j,k}} \right] \end{aligned} \quad (31)$$

248

249 The column vector  $\varphi$  is given by

250

$$\begin{aligned} \varphi = T_{i,j,k}^t + & \left( \frac{\omega\Delta t}{c_{n_{i,j,k}}\Delta x} \right) (F_{x_{i-1/2,j,k}}^t - F_{x_{i+1/2,j,k}}^t) \\ & + \left( \frac{\omega\Delta t}{c_{n_{i,j,k}}\Delta y} \right) (F_{y_{i,j-1/2,k}}^t - F_{y_{i,j+1/2,k}}^t) \\ & + \left( \frac{\omega\Delta t}{c_{n_{i,j,k}}\Delta z} \right) (F_{z_{i,j,k-1/2}}^t - F_{z_{i,j,k+1/2}}^t) \end{aligned} \quad (32)$$

251

252 The coefficients of equation (24), described in equation (25)-(32) are for an internal grid  
 253 cell with six neighbors. The coefficients for the top grid cells are modified for presence of  
 254 snow and/or standing water. A no-flux boundary condition was applied on the bottom grid  
 255 cells, thus no geothermal flux was accounted for in this study. The coefficients for the grid  
 256 cells on the lateral boundary are modified for a no-flux boundary condition. ELM handles  
 257 ice-liquid phase transitions by first predicting temperatures at the end of a time step and  
 258 then updating temperatures after accounting for deficits or excesses of energy during  
 259 melting or freezing. See Oleson (2013b) for details about the computation of thermal  
 260 properties and phase transition.

### 261 2.3.3 PETSc Numerical solution

262 ELMv0, which considers flow only in the vertical direction, solves a tridiagonal and  
 263 banded tridiagonal system of equations for water and energy transport, respectively. In  
 264 ELM-3D, accounting for lateral flow in the subsurface results in a sparse linear system,  
 265 equations (10) and (24), where the sparsity pattern of the linear system depends on grid

Gautam Bisht 11/14/2017 1:03 PM

Deleted: 24)

Gautam Bisht 11/14/2017 1:03 PM

Deleted: (25

Gautam Bisht 11/14/2017 1:02 PM

Deleted: ALM

Unknown

Field Code Changed

Gautam Bisht 11/14/2017 1:02 PM

Deleted: 2013a

Gautam Bisht 11/14/2017 1:02 PM

Deleted: ALMv0

Gautam Bisht 11/14/2017 1:02 PM

Deleted: ALM

Gautam Bisht 11/14/2017 1:03 PM

Deleted: 24)



cell connectivity. In this work, we use the PETSc (Portable, Extensible Toolkit for Scientific Computing) library (Balay et al., 2016) developed at the Argonne National Laboratory to solve the sparse linear systems. PETSc provides object-oriented data structures and solvers for scalable scientific computation on parallel supercomputers. Description about the numerical tests that were conducted to ensure the lateral coupling of hydrologic and thermal processes was correctly implemented is presented in supplementary material (Figure S 1 and S 2)

## 2.4 Snow Model and Redistribution

The snow model in [ELM](#)-3D is the same as that in the default [ELMv0](#) and CLM4.5 (Anderson, 1976; Dai and Zeng, 1997; Jordan, 1991), except for the inclusion of snow redistribution (SR). The snow model allows for a dynamic snow depth and up to five snow layers, and explicitly solves the vertically-resolved mass and energy budgets. Snow aging, compaction, and phase change are all represented in the snow model formulation. Additionally, the snow model accounts for the influence of aerosols (including black and organic carbon and mineral dust) on snow radiative transfer ([Oleson, 2013a](#)). [ELMv0](#) uses the methodology of Swenson and Lawrence (2012) to compute fractional snow cover area, which is appropriate for ESM-scale grid cells (~100 km x 100 km). Since the grid cell resolution in this work is sub-meter, we modified the fractional cover to be either 1 (when snow was present) or 0 (when snow was absent).

Two main drivers of SR include topography and surface wind (Warscher et al., 2013); previous SR models include mechanistically- (Bartelt and Lehning, 2002; Liston and Elder, 2006) and empirically- (Frey and Holzmann, 2015; Helfricht et al., 2012) based approaches. To mimic the effects of wind, we used a conceptual model to simulate SR over the fine-resolution topography of our site by instantaneously re-distributing the incoming snow flux such that lower elevation areas (polygon center) receive snow before higher elevation areas (polygon rims). This relatively simple and parsimonious approach is reasonable given the observed snow depth heterogeneity, as described below, and small spatial extent of our domain.

Gautam Bisht 11/14/2017 1:02 PM

Deleted: ALM

Gautam Bisht 11/14/2017 1:02 PM

Deleted: ALMv0

Gautam Bisht 11/14/2017 1:02 PM

Deleted: (Oleson, 2013b). ALMv0

## 304 2.5 System Characterization

305 Hydrologic and thermal properties differ by depth and landscape type. We used the  
306 horizontal distribution of organic matter (OM) content from Wainwright et al. (2015) to  
307 infer soil hydrologic and thermal properties following the default representations in [ELM](#).  
308 Vegetation cover was classified as arctic shrubs in polygon centers and arctic grasses in  
309 polygon rims. The default representation of the plant wilting factor assigns a value of zero  
310 for a given soil layer when its temperature falls below a threshold ( $T_{\text{threshold}}$ ) of  $-2^{\circ}\text{C}$ . This  
311 default value leads to overly large predicted latent and sensible heat fluxes during winter,  
312 compared to nearby eddy covariance measurements. We modified  $T_{\text{threshold}}$  to be  $0^{\circ}\text{C}$  in this  
313 study, resulting in improved predicted wintertime latent heat fluxes compared to the  
314 default version of the model (Figure S3). Although biases compared to the observations  
315 remain, particularly for sensible heat fluxes in the spring, the improvement is substantial  
316 and, given the observational uncertainties, we believe sufficient to justify our use of the  
317 model for investigations of the role of snow heterogeneity in this polygonal tundra system.

## 318 2.6 Simulation Setup, Climate Forcing, and Analyses

319 Because of computational constraints, we investigated the role of snow  
320 redistribution and physics representation using a two-dimensional transect through site A  
321 (Figure 1). The transect was 104 m long and 45 m deep and was discretized horizontally  
322 with a grid spacing of 0.25 m and an exponentially varying layer thickness in the vertical  
323 with 30 soil layers. [The transect does not align with the sensor locations because our  
324 objective was not to validate the model for a few grid cells, but to focus on relative  
325 differences between predictions for rims and centers of a polygon field.](#) No flow conditions  
326 for mass and energy were imposed on the east, west, and bottom boundaries of the domain.  
327 Temporal discretization of 30 min was used in the simulations. All simulations were  
328 performed in the “satellite phenology” (SP) mode, i.e., Leaf Area Index (LAI) was prescribed  
329 from MODIS observations.

330 Simulations were run for 10 years using long-term climate data gathered at the  
331 Barrow, Alaska Observatory site (<https://www.esrl.noaa.gov/gmd/obop/brw/>) managed  
332 by the Global Monitoring Division of NOAA’s Earth System Research Laboratory (Mefford et  
333 al., 1996). The missing precipitation time series was gap-filled using daily precipitation at

Gautam Bisht 11/14/2017 1:02 PM

Deleted: ALM

335 the Barrow Regional Airport available from the Global Historical Climatology Network  
336 (<http://www1.ncdc.noaa.gov/pub/data/ghcn/daily>). We tested the model by comparing  
337 predictions to high-frequency observations of snow depth and vertically resolved soil  
338 temperature for September 2012 – September 2013. Temperature observations were  
339 taken at discrete locations in a polygon center and rim (Figure 1), and were combined to  
340 analyze comparable landscape positions in the simulations (Figure 2).

341 After testing, the model was used to investigate the effects of snow redistribution  
342 and 2D subsurface hydrologic and thermal physics by analyzing three scenarios: (1) no  
343 snow redistribution and 1D physics; (2) snow redistribution and 1D physics; and (3) snow  
344 redistribution and 2D physics. Between these scenarios, we compared vertically-resolved  
345 soil temperature and liquid saturation, active layer depth, and mean and spatial variation of  
346 latent and sensible heat fluxes across the 10 years of simulations. For each soil column, the  
347 simulated soil temperature was interpolated vertically and the active layer depth was  
348 estimated as the maximum depth that had above-freezing soil temperature.

349 **3 Results and Discussion**

350 **3.1 Snow depth**

351 In the absence of SR, predicted snow depth exactly follows the topography. With SR,  
352 a much smaller dependence of winter-average snow depth on topography is predicted  
353 (Figure 2). Further, for the winter average, there are very small differences in snow depth  
354 between simulations with SR and 1D or 2D subsurface physics representations. Compared  
355 to observations, considering SR led to: (1) a factor of ~2 improvement in snow depth bias  
356 for the polygon center; (2) modest increase and decrease in average bias on the rims for  
357 September through February and March through June, respectively; and (3) a dramatic  
358 improvement in bias of the difference in snow depth between the polygon centers and rims  
359 (Figure 3). There was no discernible difference in snow depth bias between the 1D and 2D  
360 physics (Table 1), although the predicted subsurface temperature fields were different, as  
361 shown below.

362 The temporal variation of the mean snow depth (Figure 4a) and its spatial standard  
363 deviation (Figure 4b) also differed based on whether SR was considered, but was not

Gautam Bisht 11/14/2017 1:03 PM  
Deleted: Figure 2

Gautam Bisht 11/14/2017 1:03 PM  
Deleted: Figure 2

Gautam Bisht 11/14/2017 1:03 PM  
Deleted: Figure 3

Gautam Bisht 11/14/2017 1:03 PM  
Deleted: Table 1

Gautam Bisht 11/14/2017 1:03 PM  
Deleted: Figure 4

Gautam Bisht 11/14/2017 1:03 PM  
Deleted: Figure 4

370 affected by considering 2D thermal or hydrologic physics. With SR, the snow depth  
371 coefficient of variation (**Figure 4c**) was about 0.5 from December through the beginning of  
372 the snowmelt period, indicating relatively large spatial heterogeneity. Simulated snow  
373 depth for the three simulation scenarios are included in Supplementary Material (4)

Gautam Bisht 11/14/2017 1:03 PM  
Deleted: Figure 4

374 **3.2 Soil Temperature and Active Layer Depth**

375 Broadly, **ELM-3D** accurately predicted the polygon center soil temperature at depth  
376 intervals corresponding to the temperature probes (0-20 cm, 20-50 cm, 50-75 cm, and 75-  
377 100 cm; **Figure 5a**). Recall that the observed temperatures for the polygon center and rims  
378 were taken at single points in site A (**Figure 1**) while the predicted temperatures were  
379 calculated as averages across the transect for each of the two landscape position types. The  
380 model was able to simulate early freeze up of the soil column under the rims as compared  
381 to centers in November 2012 because of differences in accumulated snow pack. The  
382 transition to thawed soil in the 0-20 cm depth interval in early June 2013 and the  
383 subsequent temperature dynamics over the summer were very well captured by **ELM-3D**.  
384 Minimum temperatures during the winter were also accurately predicted, although the  
385 temperatures in the deepest layer (75-100 cm) were overestimated by ~3°C in March. For  
386 figure clarity we did not indicate the standard deviation of the observations, but provide  
387 that information in Supplemental Material (Figure S5-S8).

Gautam Bisht 11/14/2017 1:02 PM  
Deleted: ALM

Gautam Bisht 11/14/2017 1:03 PM  
Deleted: Figure 5

Gautam Bisht 11/14/2017 1:03 PM  
Deleted: Figure 1

388 Similarly, the soil temperatures were accurately predicted in the polygon rims  
389 (**Figure 5b**). The largest discrepancies between measured and predicted soil temperatures  
390 were in the shallowest layer (0 - 25 cm), where the predictions were up to a few °C cooler  
391 than some of the observations between December 2012 and March 2013. In the polygon  
392 center, a thicker snow pack acts as a heat insulator and keeps soil temperature higher in  
393 winter as compared to the polygon rims.

Gautam Bisht 11/14/2017 1:02 PM  
Deleted: ALM

394 Three recent studies have used other mechanistic models to simulate soil  
395 temperature fields at this site, and achieved comparably good comparisons with  
396 observations (Kumar et al. 2016 applied a 3D version of PFLOTRAN; Atchley et al. 2015 and  
397 Harp et al. 2016 applied a 1D version of ATS). However, those models used measured soil  
398 temperatures near the surface as the top boundary condition. In contrast, the top boundary  
399 condition in this work is the climate forcing (air temperature, wind, solar radiation,

Gautam Bisht 11/14/2017 1:03 PM  
Deleted: Figure 5

406 | humidity, precipitation), and the ground heat flux is prognosed based on [ELM's](#) vegetation  
407 | and surface energy dynamics. We note that no parameter calibration was done in this work  
408 | or that of Kumar et al. (2016), while the ATS parameterizations were calibrated to match  
409 | the soil temperature profile.

410 | Snow redistribution impacts spatial variability of soil temperature throughout the  
411 | soil column. Absence of SR results in no significant spatial variability of soil temperature  
412 | ([Figure 6a](#)). Inclusion of SR on the surface modifies the amount of energy exchanged  
413 | between the snow and the top soil layer, thereby creating spatial variability in the  
414 | temperature of the top soil, which propagates down into the soil column ([Figure 6b](#)). With  
415 | SR, energy dissipation in the lateral direction reduces the penetration depth of the soil  
416 | temperature spatial variance (compare [Figure 6c](#) and [Figure 6b](#)).

417 | With 1D physics, the average spatial and temporal difference of the active layer  
418 | depth (ALD) between simulations with and without SR was 1.7 cm ([Figure 7a](#)), and the  
419 | absolute difference was 6.5 cm. As described above, we diagnosed the ALD to be the  
420 | maximum soil depth during the summer at which vertically interpolated soil temperature  
421 | is 0 °C. On average, the rims had ~10 cm shallower ALD with (blue line) than without  
422 | (green line) SR, consistent with the loss of insulation from SR on the rims during the  
423 | winter. In the centers (e.g., at location 42 - 55 m), the thaw depth was deeper by ~5 cm  
424 | with SR because of the higher snow depth there from SR. The effect of SR on the ALD was  
425 | largest on the rims because, compared to centers, they (1) on average lost more snow with  
426 | SR and (2) are more thermally conductive. Since rims are therefore colder at the time of  
427 | snowmelt with SR, the ground heat flux during the subsequent summer was unable to thaw  
428 | the soil column as deeply as when SR is ignored. For comparison, Atchley et al. (2015)  
429 | found in their sensitivity analysis using the 1D version of ATS that SR resulted in deeper  
430 | thaw depths in both polygon centers (by ~3 cm) and rims (~0.3 cm). Thus, their results for  
431 | polygon centers are consistent in sign but lower in magnitude than ours, but opposite in  
432 | sign for the rims.

433 | Across ten years of simulation, the inter-annual variability (IAV) in ALD varied  
434 | substantially between the three scenarios ([Figure 7b](#)). As expected, for the 1D physics  
435 | without SR scenario (green line), the IAV in ALD was determined by landscape position  
436 | because of differences in soil and vegetation parameters. With SR and 1D physics, the

Gautam Bisht 11/14/2017 1:02 PM

Deleted: ALM's

Gautam Bisht 11/14/2017 1:03 PM

Deleted: Figure 6

Gautam Bisht 11/14/2017 1:03 PM

Deleted: Figure 6

Gautam Bisht 11/14/2017 1:03 PM

Deleted: Figure 6

Gautam Bisht 11/14/2017 1:03 PM

Deleted: Figure 6

Gautam Bisht 11/14/2017 1:03 PM

Deleted: Figure 7

Gautam Bisht 11/14/2017 1:03 PM

Deleted: Figure 7

444 model shows largest differences over the rims, again highlighting the relatively larger  
445 effects of SR on the rim soil temperatures.

446 The effect of 1D versus 2D physics on the ALD across the transect was modest  
447 (mean absolute difference  $\sim 3$  cm). Generally, because 2D physics allows for lateral energy  
448 diffusion, the horizontal variation of ALD was slightly lower (i.e., the red line is smoother  
449 than the blue line; [Figure 7a](#)) than with 1D physics. This difference was also reflected in the  
450 thaw depth IAV across the transect, where 2D physics led to a smoother lateral profile of  
451 inter-annual variability than with 1D physics.

452 The impact of physics formulation (i.e., 1D or 2D) alone was investigated by  
453 analyzing differences between soil temperature profiles over time for polygon rims and  
454 centers in simulations with snow redistribution. Inclusion of 2D subsurface physics  
455 resulted in soil temperatures with depth and time that were lower in the polygon rims  
456 ([Figure 8a](#)) and higher in polygon centers ([Figure 8b](#)). Using the simulations from the  
457 scenario with SR and 2D physics, we evaluated the extent to which soils under rims and  
458 centers can be separately considered as relatively homogeneous single column systems by  
459 evaluating the soil temperature standard deviation as a function of depth and time ([Figure](#)  
460 [9](#)). During winter, both polygon rims and centers were predicted to have soil temperature  
461 spatial variability  $>1$  °C up to a depth of  $\sim 2$  m. The soil temperature spatial variability in  
462 winter due to snow redistribution was dissipated over the summer. During the summer,  
463 polygon centers were relatively more homogeneous vertically compared to polygon rims.

### 464 3.3 Surface Energy Budget

465 Predicted monthly- and spatial-mean ( $\mu$ ) surface latent heat fluxes across the  
466 transect were very similar between the three scenarios ([Figure 10a](#)), with a growing  
467 seasonal mean difference of  $< 1.0$  W m<sup>-2</sup>. However, the spatial variability ( $SV = \sigma$ ; [Figure](#)  
468 [10b](#)) and coefficient of variation ( $CV = \sigma/\mu$ ; [Figure 10c](#)) of latent heat fluxes were different  
469 between the scenarios with SR (1D and 2D physics) and without SR. With SR, the latent  
470 heat flux spatial standard deviation peaked after snowmelt and declined until the fall when  
471 snow began, from about  $\sim 100\%$  to  $10\%$  of the mean. This relatively larger spatial variation  
472 in latent heat flux occurred because of large spatial heterogeneity in near surface soil

Gautam Bisht 11/14/2017 1:03 PM  
Deleted: Figure 7

Gautam Bisht 11/14/2017 1:03 PM  
Deleted: Figure 8

Gautam Bisht 11/14/2017 1:03 PM  
Deleted: Figure 8

Gautam Bisht 11/14/2017 1:03 PM  
Deleted: Figure 9

Gautam Bisht 11/14/2017 1:03 PM  
Deleted: Figure 10

Gautam Bisht 11/14/2017 1:03 PM  
Deleted: Figure 10

Gautam Bisht 11/14/2017 1:03 PM  
Deleted: Figure 10

480 moisture in the beginning of summer, indicating a residual effect of SR from the previous  
481 winter.

482 The predicted temporal monthly-mean and spatial-mean surface sensible heat  
483 fluxes across the transect were also similar between the three scenarios (Figure 11a), with  
484 a growing season mean absolute difference of  $< 3.5 \text{ W m}^{-2}$ . Also, the sensible heat flux  
485 spatial variability differences occurred earlier than snowmelt, in contrast to the latent heat  
486 flux. Both the standard deviation and CV of the sensible heat fluxes were larger than those  
487 of the latent heat fluxes, with early season standard deviations of  $\sim 50 \text{ W m}^{-2}$  (Figure 11b)  
488 and CV's of  $\sim 1.5$  (Figure 11c). As for the latent heat fluxes, the differences in standard  
489 deviation and CV of sensible heat fluxes were small between the 1D and 2D scenarios with  
490 SR, arguing that the subsurface lateral energy exchanges associated with the 2D physics did  
491 not propagate to the mean surface heat fluxes. However, as for the latent heat flux, there  
492 was a relatively large difference in spatial variation between the scenarios with and  
493 without SR (e.g., of about  $25 \text{ W m}^{-2}$  in May; Figure 10b).

494 **3.4 Soil Moisture**

495 Neither SR nor 2D lateral physics affected the spatial mean moisture across time  
496 (not shown). However, spatial heterogeneity of predicted soil moisture content differed  
497 substantially between scenarios during the snow free period (Figure 12). For the 1D  
498 simulations, the effect of SR was to increase growing season soil moisture spatial  
499 heterogeneity by factors of 5.2 and 1.6 for 0-10 cm and 10-65 cm depth intervals,  
500 respectively (compare Figure 12a and Figure 12b). Compared to 1D physics, simulating 2D  
501 thermal and hydrologic physics led to an overall reduction in soil moisture spatial  
502 heterogeneity by factors of 0.8 and 0.7 for 0-10 cm and 10-65 cm depth intervals,  
503 respectively (compare Figure 12b and Figure 12c). Thus, with respect to dynamic spatial  
504 mean soil moisture, SR effects dominated those associated with lateral subsurface water  
505 movement.

506 **3.5 Caveats and Future Work**

507 The good agreement between ELM-3D predictions and soil temperature  
508 observations demonstrate the model's capabilities to represent this very spatially

Gautam Bisht 11/14/2017 1:03 PM  
Deleted: Figure 11

Gautam Bisht 11/14/2017 1:03 PM  
Deleted: Figure 11

Gautam Bisht 11/14/2017 1:03 PM  
Deleted: Figure 11

Gautam Bisht 11/14/2017 1:03 PM  
Deleted: Figure 10

Gautam Bisht 11/14/2017 1:03 PM  
Deleted: Figure 12

Gautam Bisht 11/14/2017 1:03 PM  
Deleted: Figure 12

Gautam Bisht 11/14/2017 1:03 PM  
Deleted: Figure 12

Gautam Bisht 11/14/2017 1:03 PM  
Deleted: Figure 12

Gautam Bisht 11/14/2017 1:03 PM  
Deleted: Figure 12

Gautam Bisht 11/14/2017 1:02 PM  
Deleted: ALM

519 heterogeneous and complex system. However, several caveats to our conclusions remain  
520 due to uncertainties in model parameterizations, model structure, and climate forcing data.

521 ELMv0, a one-dimensional model, is embarrassing parallel with no cross processor  
522 communication. The current implementation of the three-dimensional solver in ELM-3D  
523 only supports serial computing. Support of parallel computing will be included in a future  
524 version of the model. Because of computational constraints, we applied a 2D transect  
525 domain to the site, instead of a full 3D domain. We are working to improve the  
526 computational efficiency of the model, which will facilitate a thorough analysis of the  
527 effects of 3D subsurface energy and water fluxes. A related issue is our simplified treatment  
528 of surface water flows. A thorough analysis of the effects of surface water redistribution  
529 would require integration of a 2D surface thermal flow model in a 3D domain, which is  
530 another goal for our future work. However, we note that the good agreement using the 2D  
531 model domain supports the idea that a two-dimensional simplification may be appropriate  
532 for this system. The expected geomorphological changes in these systems over the coming  
533 decades (e.g., Liljedahl et al. 2016), which will certainly affect soil temperature and  
534 moisture, are not currently represented in ELM, although incorporation of these processes  
535 is a long-term development goal.

536 The current representation of vegetation in ELM-3D for these polygonal tundra  
537 systems is over-simplified. For example, non-vascular plants (mosses and lichens) are not  
538 explicitly represented in the model, but can be responsible for a majority of evaporative  
539 losses (Miller et al., 1976) and are strongly influenced by near surface hydrologic  
540 conditions (Williams and Flanagan, 1996). Our use of the 'satellite phenology' mode, which  
541 imposes transient LAI profiles for each plant functional type in the domain, ignores the  
542 likely influence of nutrient constraints (Zhu et al., 2016) on photosynthesis and therefore  
543 the surface energy budget. Other model simplifications, e.g., the simplified treatment of  
544 radiation competition may also be important, especially as simulations are extended over  
545 periods where vegetation change may occur (e.g., Grant 2016).

546 Development of sub grid parameterizations to parsimoniously capture fine scale  
547 processes will be pursued in the future. For example, a two-tile approach to represent  
548 hydrologic and thermal processes in coupled polygon rims and centers with snow  
549 redistribution should be evaluated. Inclusion of lateral subsurface processes has a greater

Gautam Bisht 11/14/2017 1:02 PM  
Deleted: ALMv0

Gautam Bisht 11/14/2017 1:02 PM  
Deleted: ALM

Gautam Bisht 11/14/2017 1:02 PM  
Deleted: ALM

Gautam Bisht 11/14/2017 1:02 PM  
Deleted: ALM



554 impact on predicted subgrid variability than on spatially averaged states. Thus, one  
 555 possible extension of the current model would be to explicitly include an equation for the  
 556 temporal evolution of sub grid variability using the approach of Montaldo and Albertson  
 557 (2003). The use of reduced-order models (e.g., Pau et al. (2014); Liu et al. (2016)) is an  
 558 alternate approach to estimate fine scale hydrologic and thermal states from a coarse  
 559 resolution representation. Additionally, lateral subsurface processes can be included in the  
 560 land surface model via a range of numerical discretization approaches of varying  
 561 complexity, e.g., adding lateral water and energy fluxes as source/sink terms in the existing  
 562 1D model, implementing an operator split approach to solve vertical and lateral processes  
 563 in a non-iterative approach, or solving a fully coupled 3D model. Tradeoffs between  
 564 approaches that represent lateral processes and computational costs need to be carefully  
 565 studied before developing quasi or fully three-dimensional land surface models. While the  
 566 present study focused on application and validation of ELM-3D at fine-scale, future work  
 567 will focus on regional scale applications using comprehensive datasets and the Distributed  
 568 Model Intercomparison Project Phase 2 modeling protocol (Smith et al., 2012). Although  
 569 we found no significant effect of topography and SR on the 100 m × 100 m grid-averaged  
 570 exchanges with the atmosphere, future work needs to analyze intermediate scale (e.g., 100  
 571 m – 10 km) topographical variation and the potential effects on biogeochemical and plant  
 572 processes and surface exchanges.

## 573 4 Summary and Conclusions

574 In a polygonal tundra landscape, we analyzed effects of microtopographical surface  
 575 heterogeneity and lateral subsurface transport on soil temperature, soil moisture, and  
 576 surface energy exchanges. Starting from the climate-scale land model ELMv0, we  
 577 incorporated in ELM-3D numerical representations of subsurface water and energy lateral  
 578 transport that are solved using PETSc. A simple method for redistributing incoming snow  
 579 along the microtopographic transect was also integrated in the model.

580 Over the observational record, ELM-3D with snow redistribution and lateral heat  
 581 and hydrological fluxes accurately predicted snow depth and soil temperature vertical  
 582 profiles in the polygon rims and centers (overall bias, RMSE, and  $R^2$  of 0.59°C, 1.82°C and

Gautam Bisht 11/14/2017 1:02 PM

Deleted: various

Gautam Bisht 11/14/2017 1:02 PM

Deleted: to include

Gautam Bisht 11/14/2017 1:02 PM

Deleted: needs

Gautam Bisht 11/14/2017 1:02 PM

Deleted: ALM

Gautam Bisht 11/14/2017 1:02 PM

Deleted: modeling protocol of

Gautam Bisht 11/14/2017 1:02 PM

Deleted: ALMv0

Gautam Bisht 11/14/2017 1:02 PM

Deleted: ALM

Gautam Bisht 11/14/2017 1:02 PM

Deleted: ALM

591 0.99, respectively). In the rims, the transition to thawed soil in spring, summer  
592 temperature dynamics, and minimum temperatures during the winter were all accurately  
593 predicted. In the centers, a  $\sim 2^{\circ}\text{C}$  warm bias in April in the 75-100 cm soil layer was  
594 predicted, although this bias disappeared during snowmelt.

595 The spatial heterogeneity of snow depth during the winter due to snow  
596 redistribution generated surface soil temperature heterogeneity that propagated into the  
597 soil over time. The temporal and spatial variation of snow depth was affected by snow  
598 redistribution, but not by lateral thermal and hydrologic transport. Both snow  
599 redistribution and lateral thermal fluxes affected spatial variability of soil temperatures.  
600 Energy dissipation in the lateral direction reduced the depth to which soil temperature  
601 variance penetrated. Snow redistribution led to  $\sim 10$  cm shallower active layer depths  
602 under the polygon rims because of the residual effect of reduced insulation during the  
603 winter. In contrast, snow redistribution led to  $\sim 5$  cm deeper maximum thaw depth under  
604 the polygon centers. The effect of lateral energy fluxes on active layer depths was  $\sim 3$  cm.  
605 Compared to 1D physics, the 2D subsurface physics led to lower (higher) soil temperatures  
606 with depth and time in the polygon rims (centers). The larger than  $1^{\circ}\text{C}$  wintertime spatial  
607 temperature variability down to  $\sim 2$  m depth in rims and centers indicates the uncertainty  
608 associated with considering rims and centers as separate 1D columns. During the summer,  
609 polygon center temperatures were relatively more vertically homogeneous than  
610 temperatures in the rims.

611 The monthly- and spatial-mean predicted latent and sensible heat fluxes were  
612 unaffected by snow redistribution and lateral heat and hydrological fluxes. However, snow  
613 redistribution led to spatial heterogeneity in surface energy fluxes and soil moisture during  
614 the summer. Excluding lateral subsurface hydrologic and thermal processes led to an over  
615 prediction of spatial variability in soil moisture and soil temperature because subsurface  
616 gradients were artificially prevented from laterally dissipating over time. Snow  
617 redistribution effects on soil moisture heterogeneity were larger than those associated  
618 with lateral thermal fluxes.

619 Overall, our analysis demonstrates the potential and value of explicitly representing  
620 snow redistribution and lateral subsurface hydrologic and thermal dynamics in polygonal  
621 ground systems and quantifies the effects of these processes on the resulting system states

522 and surface energy exchanges with the atmosphere. The integration of a 3D subsurface  
523 | model in the E3SM Land Model also allows for a wide range of analyses heretofore  
524 impossible in an Earth System Model context.

525

Gautam Bisht 11/14/2017 1:02 PM

**Deleted:** ACME

527 **5 Code availability**

528 | The ELM-3D v1.0 code and data used in study are publicly available at

529 <https://bitbucket.org/gbisht/lateral-subsurface-model> and

530 <https://bitbucket.org/gbisht/notes-for-gmd-2017-71>.

531

Gautam Bisht 11/14/2017 1:02 PM

Deleted: ALM

533 **6 Tables**

534 **Table 1. Bias, root mean square error (RMSE), and correlation ( $R^2$ ) between modeled and**  
535 **observed snow depth at polygon center, rim and difference between center and rim for**  
536 **2013 for three cases: Snow redistribution (SR) off and 1D physics, SR on and 1D physics,**  
537 **and SR on and 2D physics.**

|       | SR=Off, Physics=1D |      |                | SR=On, Physics=1D |       |                | SR=On, Physics=2D |       |                |
|-------|--------------------|------|----------------|-------------------|-------|----------------|-------------------|-------|----------------|
|       | Center             | Rim  | Center-<br>Rim | Center            | Rim   | Center-<br>Rim | Center            | Rim   | Center-<br>Rim |
| Bias  | -0.08              | 0.02 | -0.10          | -0.04             | -0.03 | -0.02          | -0.04             | -0.03 | -0.02          |
| RMSE  | 0.12               | 0.04 | 0.12           | 0.08              | 0.04  | 0.05           | 0.08              | 0.04  | 0.05           |
| $R^2$ | 0.86               | 0.92 | 0.03           | 0.78              | 0.85  | 0.73           | 0.79              | 0.85  | 0.73           |

538

539

540 **Table 2 Bias, root mean square error (RMSE) and correlation ( $R^2$ ) between modeled and**  
541 **observed soil temperature at polygon center and rim at multiple soil depth for 2013 for**  
542 **three cases: Snow redistribution (SR) off and 1D physics, SR on and 1D physics, and SR on**  
543 **and 2D physics.**

| Bias                       |                    |       |                   |       |                   |      |
|----------------------------|--------------------|-------|-------------------|-------|-------------------|------|
|                            | SR=Off, Physics=1D |       | SR=On, Physics=2D |       | SR=On, Physics=2D |      |
| Depth [m]                  | Center             | Rim   | Center            | Rim   | Center            | Rim  |
| 0.00 - 0.20                | 0.86               | -1.73 | -0.19             | 1.00  | 0.52              | 0.71 |
| 0.20 - 0.50                | 0.68               | -1.52 | -0.46             | 0.98  | 0.35              | 0.62 |
| 0.50 - 0.75                | 0.53               | -1.49 | -0.64             | 0.94  | 0.21              | 0.53 |
| 0.75 - 1.00                | 0.49               | -1.44 | -0.67             | -0.97 | 0.22              | 0.49 |
| Average across four depths | 0.64               | -1.54 | -0.49             | 0.97  | 0.33              | 0.59 |

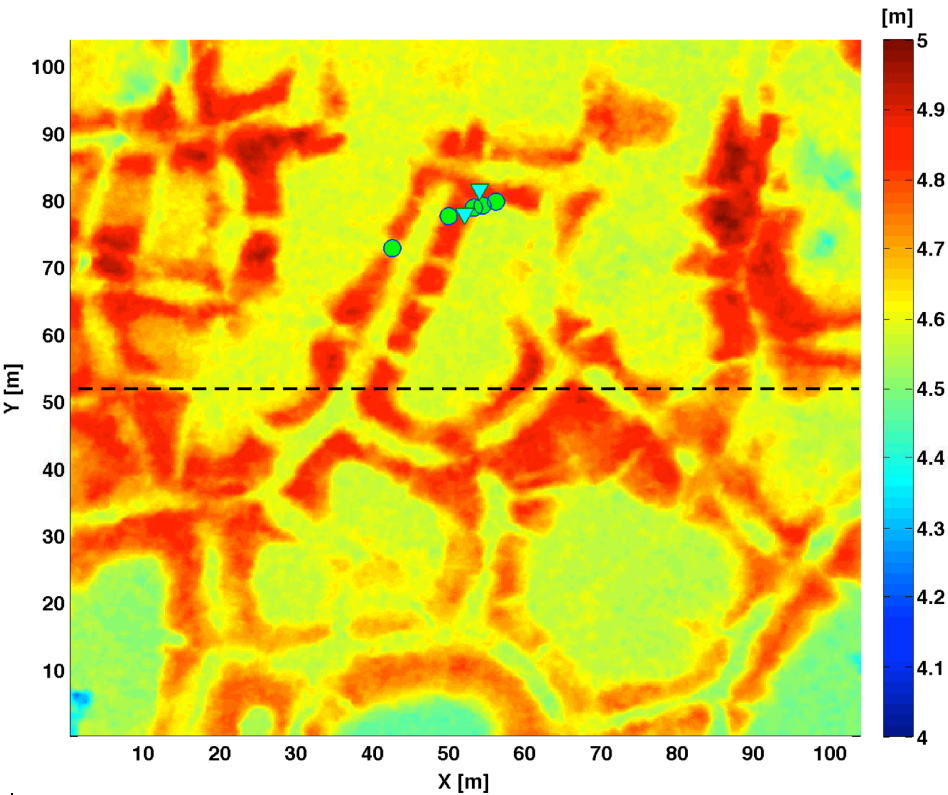
| RMSE                       |                    |      |                   |      |                   |      |
|----------------------------|--------------------|------|-------------------|------|-------------------|------|
|                            | SR=Off, Physics=1D |      | SR=On, Physics=2D |      | SR=On, Physics=2D |      |
| Depth [m]                  | Center             | Rim  | Center            | Rim  | Center            | Rim  |
| 0.00 - 0.20                | 2.11               | 3.39 | 2.20              | 2.94 | 1.90              | 2.66 |
| 0.20 - 0.50                | 1.49               | 2.73 | 1.39              | 1.86 | 1.12              | 1.57 |
| 0.50 - 0.75                | 1.60               | 2.42 | 1.22              | 1.96 | 1.14              | 1.60 |
| 0.75 - 1.00                | 1.50               | 2.15 | 1.12              | 1.87 | 1.09              | 1.44 |
| Average across four depths | 1.67               | 2.67 | 1.44              | 2.16 | 1.31              | 1.82 |

| $R^2$       |                    |      |                   |      |                   |      |
|-------------|--------------------|------|-------------------|------|-------------------|------|
|             | SR=Off, Physics=1D |      | SR=On, Physics=2D |      | SR=On, Physics=2D |      |
| Depth [m]   | Center             | Rim  | Center            | Rim  | Center            | Rim  |
| 0.00 - 0.20 | 0.98               | 0.95 | 0.97              | 0.97 | 0.98              | 0.97 |

|                                  |      |      |      |      |      |      |
|----------------------------------|------|------|------|------|------|------|
| 0.20 - 0.50                      | 0.99 | 0.96 | 0.98 | 0.99 | 0.99 | 0.99 |
| 0.50 - 0.75                      | 0.99 | 0.97 | 0.99 | 0.99 | 1.00 | 0.99 |
| 0.75 - 1.00                      | 0.99 | 0.97 | 0.99 | 0.99 | 1.00 | 0.99 |
| Average<br>across four<br>depths | 0.99 | 0.96 | 0.98 | 0.99 | 0.99 | 0.99 |

547

548 **7 Figures**

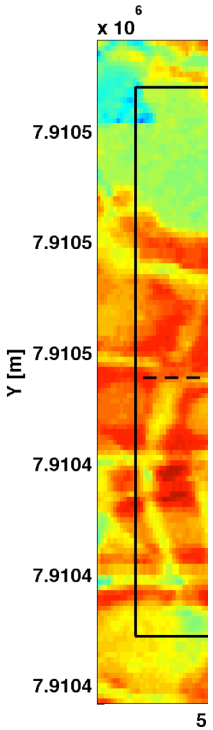


549

550 **Figure 1** The NGEE-Arctic study area A, which characterized as a low-centered polygon  
551 **field.** Dotted line indicate the transect along which simulation in this paper are preformed  
552 **to demonstrate the effects of snow redistribution on soil temperature.** The locations where  
553 **snow and temperature sensors are installed within the study site are denoted by triangle**  
554 **and circle, respectively.**

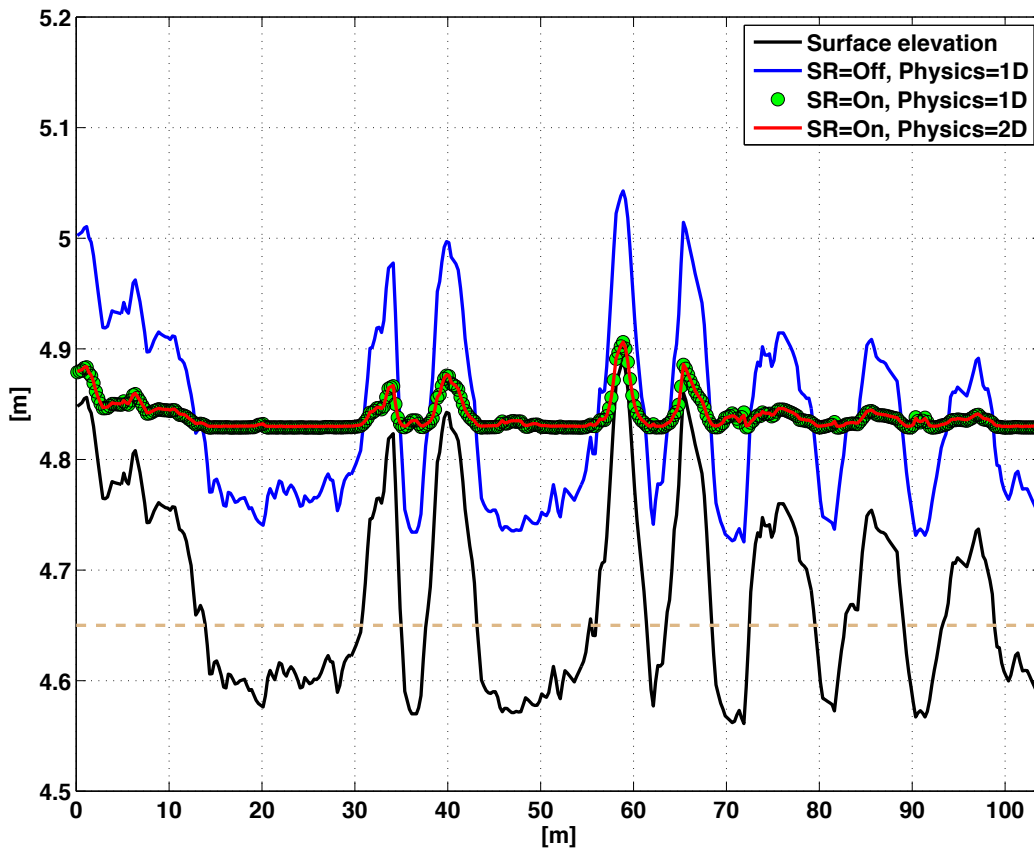
555

Gautam Bisht 11/14/2017 1:02 PM



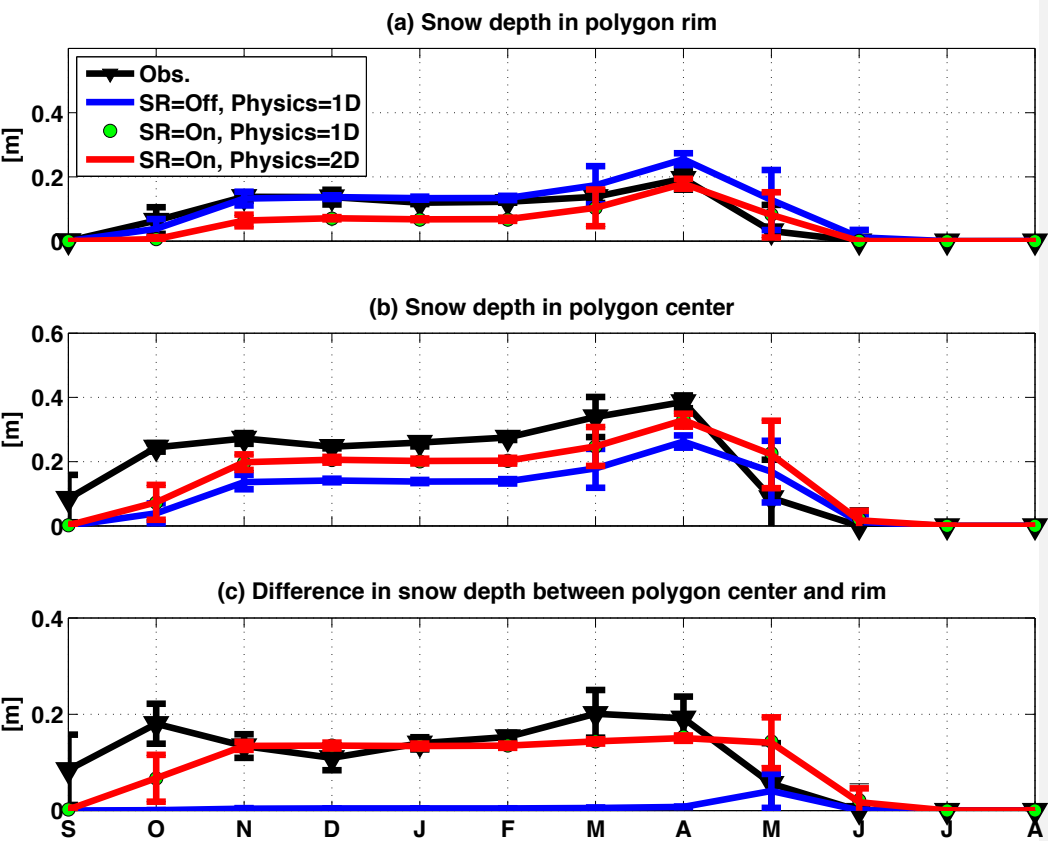
Deleted:





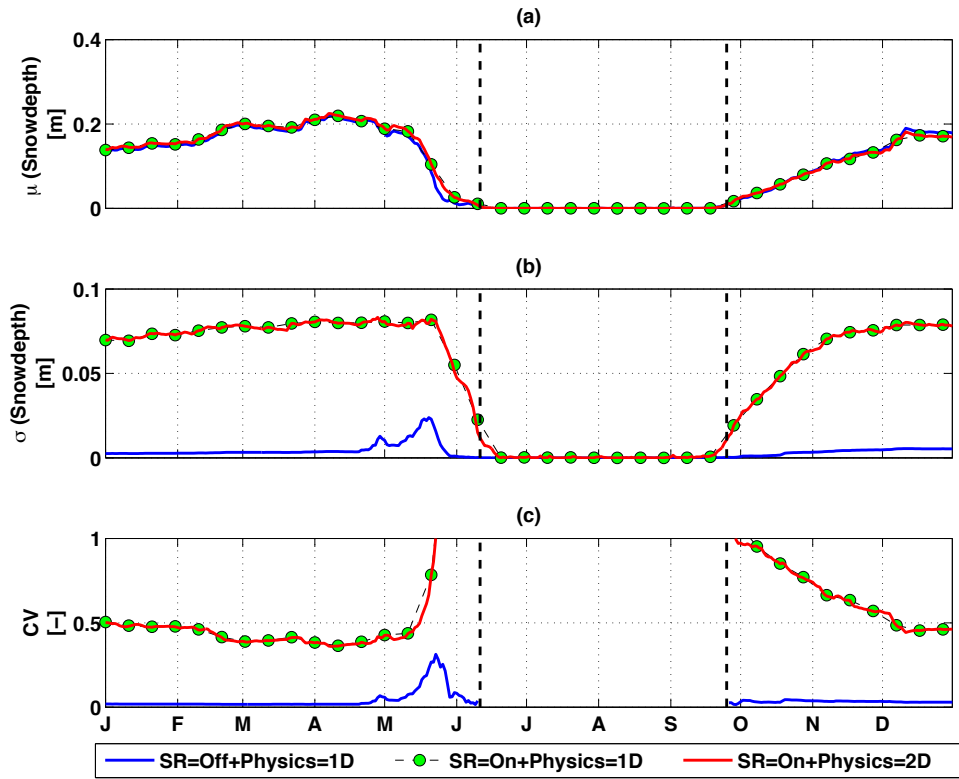
557  
 558 **Figure 2. Simulated average winter snow surface elevation across the transect for three**  
 559 **scenarios: (1) snow redistribution (SR) turned off and 1D subsurface physics, (2) snow**  
 560 **redistribution turned on and 1D subsurface physics, and (3) snow redistribution turned on**  
 561 **and 2D subsurface physics. Surface elevation of the transect is shown by solid black line.**  
 562 **The dashed line indicates the boundary for comparison to observations in relatively lower**  
 563 **(centers) and relatively higher (rims) topographical positions.**

564  
565

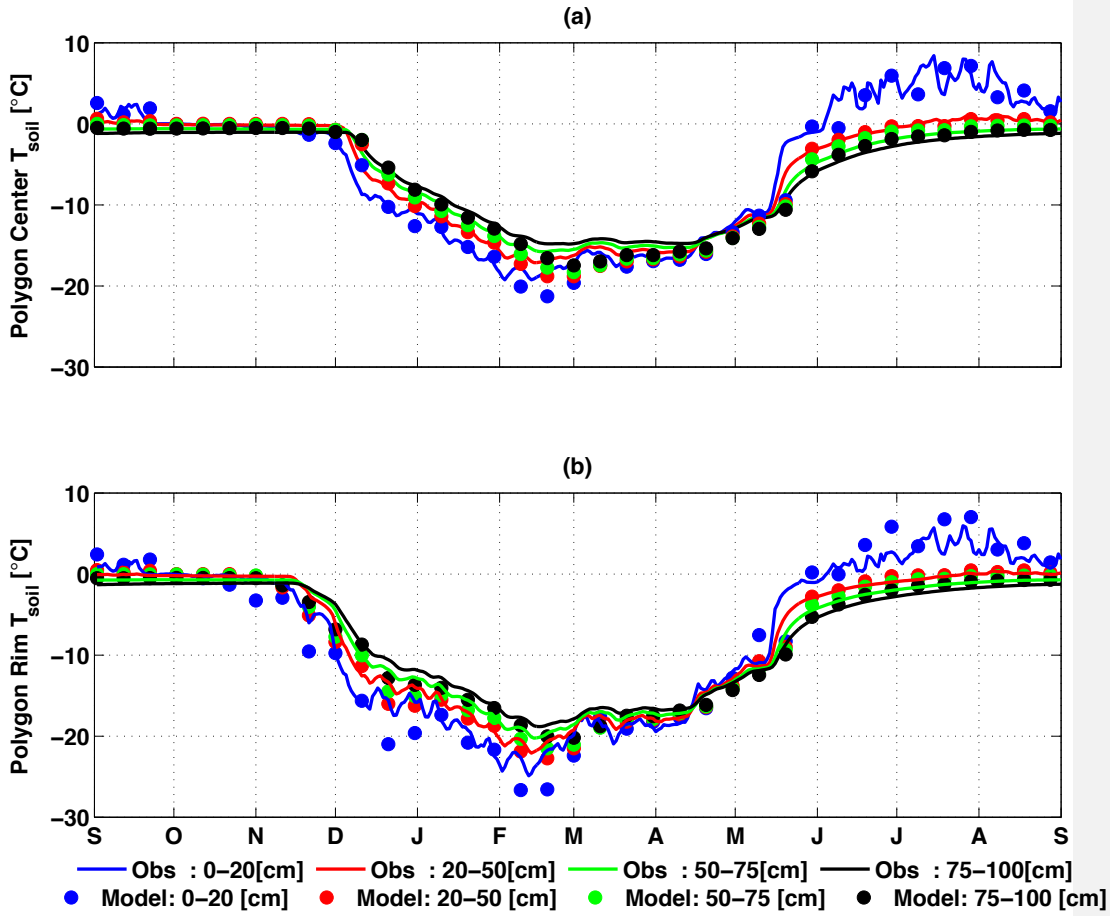


566  
567

568 **Figure 3** Monthly-mean comparison of observation and simulated snow depth (a) in  
569 polygon rim, (b) in polygon center; (c) difference between polygon center and rim for 2013.

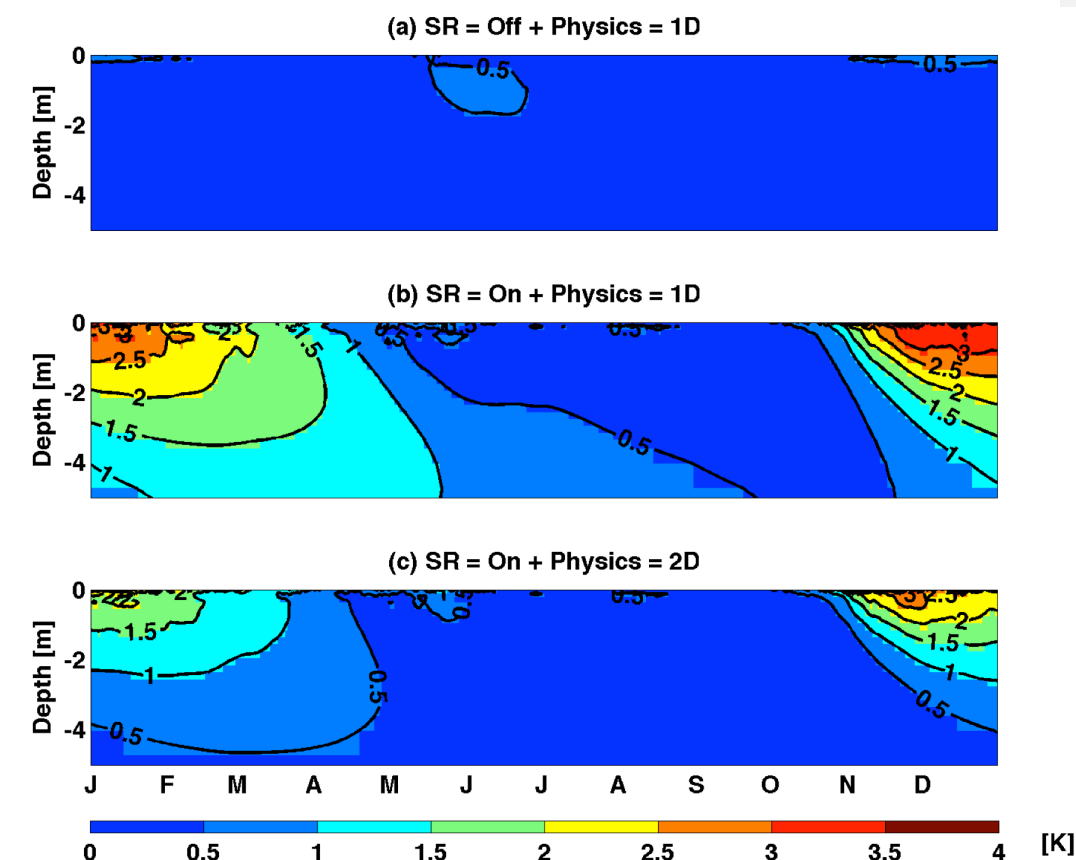


570  
 571 | **Figure 4. (a) Mean, (b) standard deviation and (c) coefficient of variation of**  
 572 **simulated snow depth across the entire domain for 1D and 2D subsurface physics.**



573  
 574 **Figure 5 Comparison of soil temperature observations and predictions in polygon centers**  
 575 **(a) and rims (b). Simulation was performed with snow redistribution on and 2D subsurface**  
 576 **physics, between September 2012 and September 2013. Simulation results are shown at an**  
 577 **interval of 10 days, while observations are shown at daily interval**

578  
 579



580  
 581 | Figure 6 Simulated daily spatial standard deviation for each soil layer averaged across 10-  
 582 year of near surface soil temperature for simulation performed with snow redistribution  
 583 turned off and 1D subsurface physics (top panel); snow redistribution turned on and 1D  
 584 subsurface physics (middle panel); and snow redistribution turned on and 2D subsurface  
 585 physics (bottom panel).

586  
 587

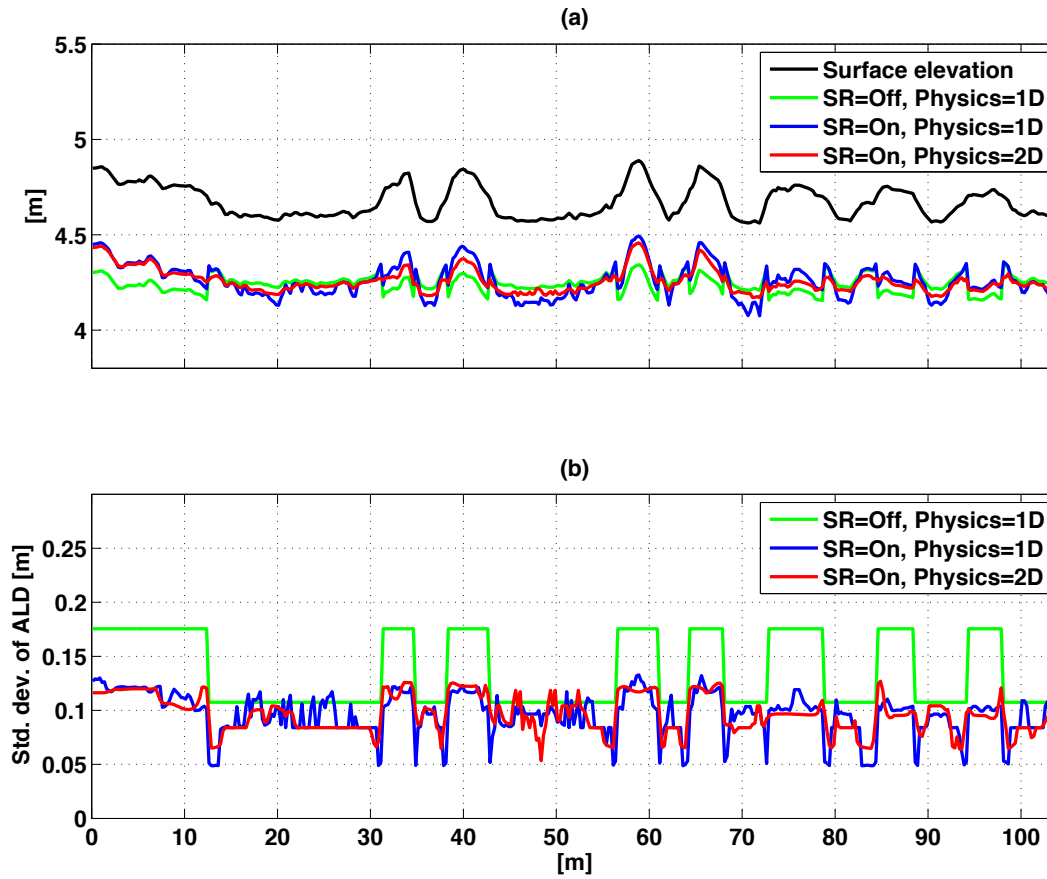
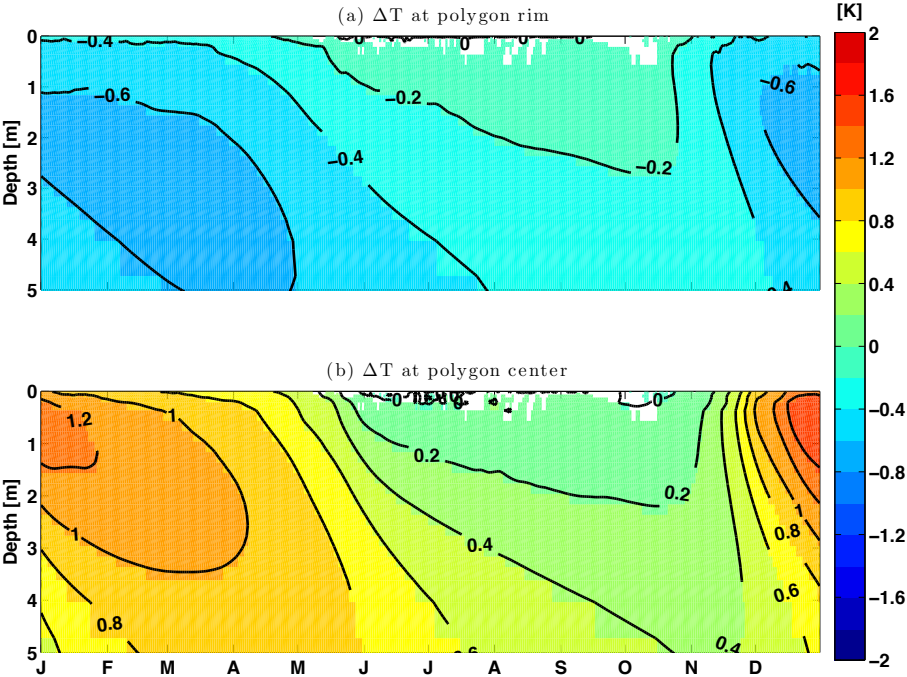
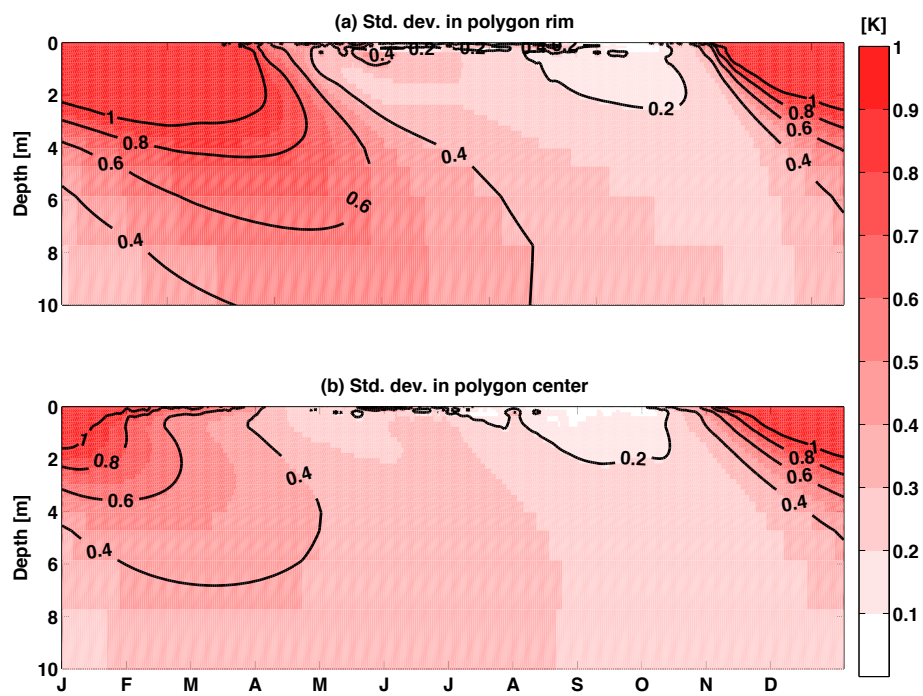


**Figure 7** Temporal mean of the bottom of the active layer (top panel) and standard deviation of the active layer depth (bottom panel) over the 10-year period across the modeling domain.

594  
595



596  
597 **Figure 8** Time series of spatial mean soil temperature differences between “SR=On +  
598 **Physics=1D**” and “SR=On + Physics=2D” at polygon rim (top panel) and polygon center  
599 (bottom panel).



700  
 701 **Figure 9** Time series of soil temperature spatial standard deviation for “SR=On +  
 702 **Physics=2D”** at polygon rim (top panel) and polygon center (bottom panel).



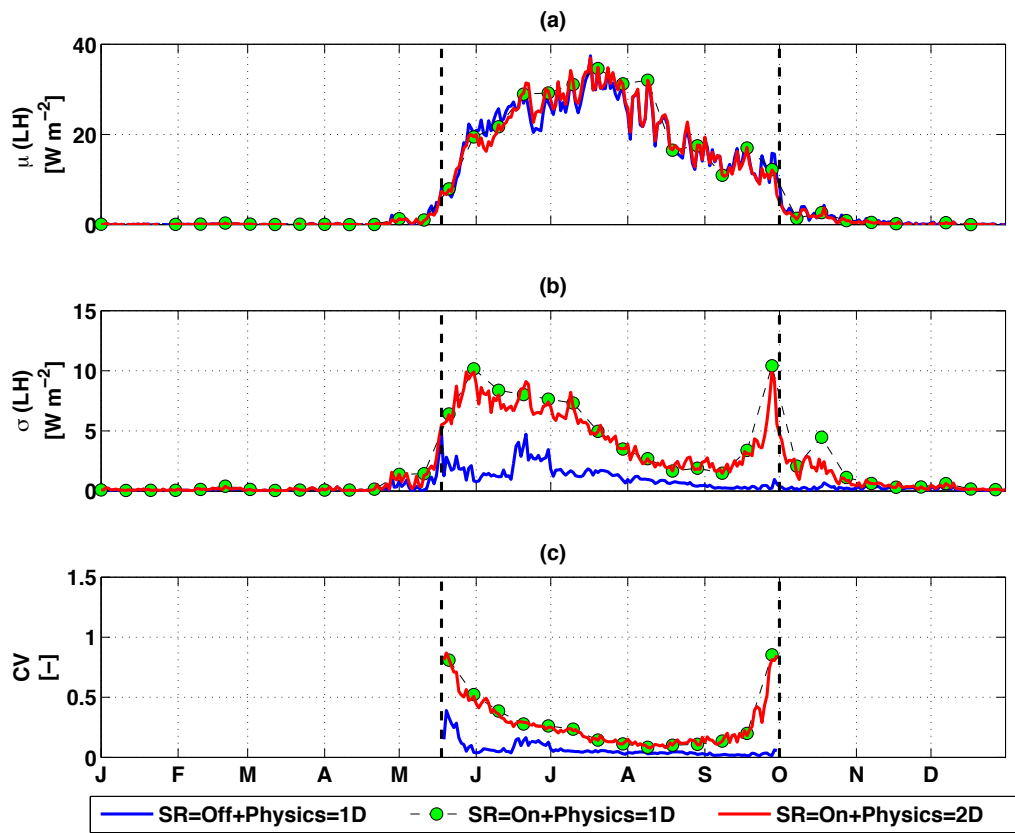


Figure 10. Latent heat flux inter-annual (a) mean, (b) standard deviation, and (c) coefficient of variation across the site A transect.

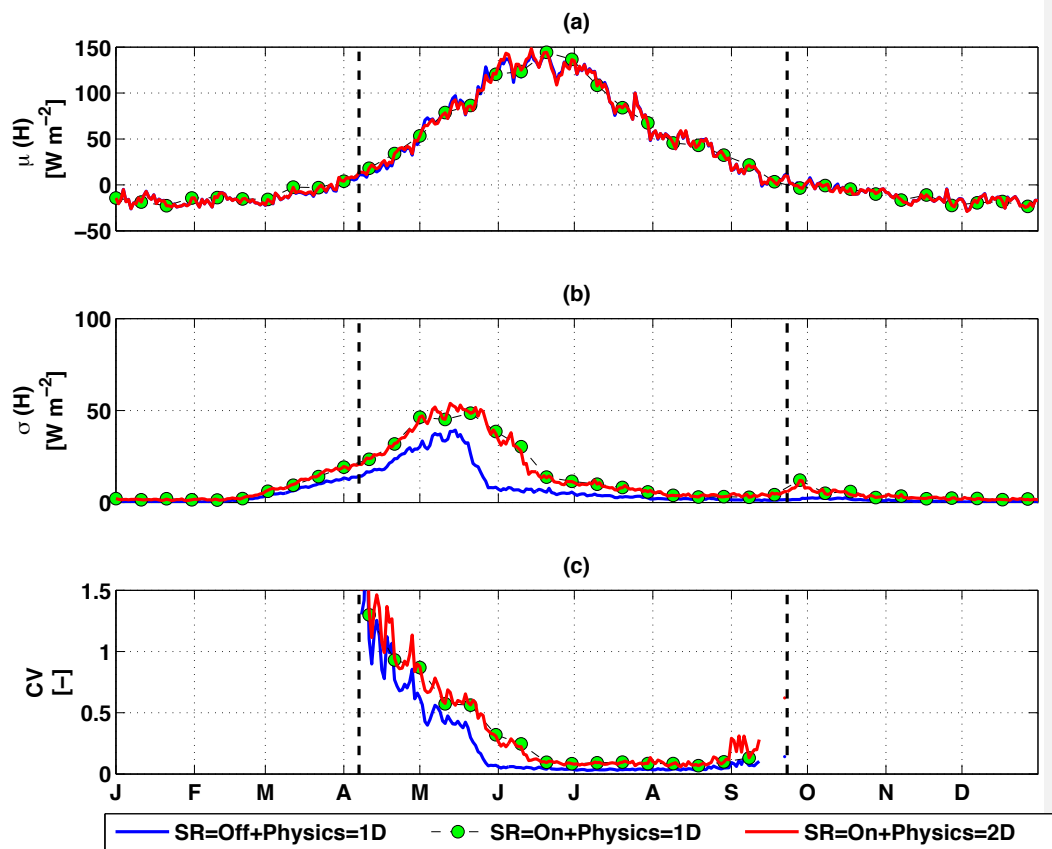
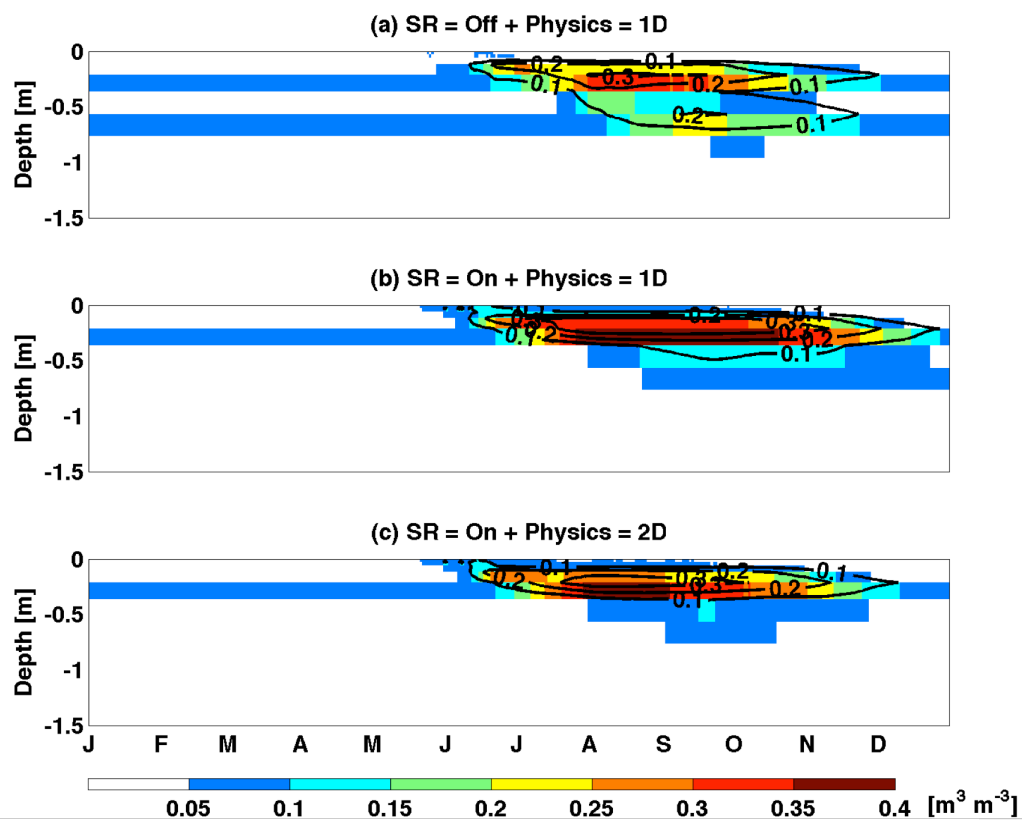


Figure 11. Same as Figure 10 except for sensible heat flux.

Gautam Bisht 11/14/2017 1:03 PM  
 Deleted: Figure 10



713

714 | Figure 12. Same as Figure 6 except for liquid saturation.

Gautam Bisht 11/14/2017 1:03 PM

Deleted: Figure 6

716 **Acknowledgements.**  
717 This research was supported by the Director, Office of Science, Office of Biological and  
718 Environmental Research of the US Department of Energy under Contract No. DE-AC02-  
719 05CH11231 as part of the NGEE-Arctic and Energy Exascale Earth System Model (E3SM)  
720 programs.

Gautam Bisht 11/14/2017 1:02 PM  
**Deleted:** Accelerated Climate Modeling for

Gautam Bisht 11/14/2017 1:02 PM  
**Deleted:** (ACME

723 **References**

- 724 Anderson, E. A.: A point energy and mass balance model of a snow cover, National Weather  
 725 Service, Silver Spring, MD, 1976.
- 726 Balay, S., Abhyankar, S., Adams, M. F., Brown, J., Brune, P., Buschelman, K., Dalcin, L.,  
 727 Eijkhout, V., Gropp, W. D., Kaushik, D., Knepley, M. G., McInnes, L. C., Rupp, K., Smith, B.  
 728 F., Zampini, S., Zhang, H., and Zhang, H.: PETSc Users Manual, Argonne National Laboratory,  
 729 2016.
- 730 Bartelt, P. and Lehning, M.: A physical SNOWPACK model for the Swiss avalanche warning:  
 731 Part I: numerical model, Cold Regions Science and Technology, 35, 123-145, 2002.
- 732 Borner, A. P., Kielland, K., and Walker, M. D.: Effects of Simulated Climate Change on Plant  
 733 Phenology and Nitrogen Mineralization in Alaskan Arctic Tundra, Arctic, Antarctic, and Alpine  
 734 Research, 40, 27-38, 2008.
- 735 Callaghan, T., Johansson, M., Brown, R., Groisman, P., Labba, N., Radionov, V., Barry, R.,  
 736 Bulygina, O., Essery, R. H., Frolov, D. M., Golubev, V., Grenfell, T., Petrushina, M., Razuvaev,  
 737 V., Robinson, D., Romanov, P., Shindell, D., Shmakin, A., Sokratov, S., Warren, S., and Yang,  
 738 D.: The Changing Face of Arctic Snow Cover: A Synthesis of Observed and Projected Changes,  
 739 AMBIO, 40, 17-31, 2011a.
- 740 Callaghan, T., Johansson, M., Brown, R., Groisman, P., Labba, N., Radionov, V., Bradley, R.,  
 741 Blangy, S., Bulygina, O., Christensen, T., Colman, J., Essery, R. H., Forbes, B., Forchhammer,  
 742 M., Golubev, V., Honrath, R., Juday, G., Meshcherskaya, A., Phoenix, G., Pomeroy, J., Rautio,  
 743 A., Robinson, D., Schmidt, N., Serreze, M., Shevchenko, V., Shiklomanov, A., Shmakin, A.,  
 744 Sköld, P., Sturm, M., Woo, M.-k., and Wood, E.: Multiple Effects of Changes in Arctic Snow  
 745 Cover, AMBIO, 40, 32-45, 2011b.
- 746 Clark, M. P., Hendrikx, J., Slater, A. G., Kavetski, D., Anderson, B., Cullen, N. J., Kerr, T., Örn  
 747 Hreinsson, E., and Woods, R. A.: Representing spatial variability of snow water equivalent in  
 748 hydrologic and land-surface models: A review, Water Resources Research, 47, W07539, 2011.
- 749 Cox, P. M., Betts, R. A., Jones, C. D., Spall, S. A., and Totterdell, I. J.: Acceleration of global  
 750 warming due to carbon-cycle feedbacks in a coupled climate model, Nature, 408, 184-187, 2000.
- 751 Dai, Y. and Zeng, Q.: A land surface model (IAP94) for climate studies part I: Formulation and  
 752 validation in off-line experiments, Advances in Atmospheric Sciences, 14, 433-460, 1997.

753 Dufresne, J. L., Fairhead, L., Le Treut, H., Berthelot, M., Bopp, L., Ciais, P., Friedlingstein, P.,  
 754 and Monfray, P.: On the magnitude of positive feedback between future climate change and the  
 755 carbon cycle, *Geophysical Research Letters*, 29, 43-41-43-44, 2002.  
 756 Engstrom, R., Hope, A., Kwon, H., Stow, D., and Zanolodchikov, D.: Spatial distribution of  
 757 near surface soil moisture and its relationship to microtopography in the Alaskan Arctic coastal  
 758 plain, *Nordic Hydrology*, 36, 219-234, 2005.  
 759 Euskirchen, E. S., McGuire, A. D., Chapin, F. S., Yi, S., and Thompson, C. C.: Changes in  
 760 vegetation in northern Alaska under scenarios of climate change, 2003–2100: implications for  
 761 climate feedbacks, *Ecological Applications*, 19, 1022-1043, 2009.  
 762 Frey, S. and Holzmann, H.: A conceptual, distributed snow redistribution model, *Hydrol. Earth*  
 763 *Syst. Sci.*, 19, 4517-4530, 2015.  
 764 Friedlingstein, P., Bopp, L., Ciais, P., Dufresne, J.-L., Fairhead, L., LeTreut, H., Monfray, P.,  
 765 and Orr, J.: Positive feedback between future climate change and the carbon cycle, *Geophysical*  
 766 *Research Letters*, 28, 1543-1546, 2001.  
 767 Friedlingstein, P., Cox, P., Betts, R., Bopp, L., von Bloh, W., Brovkin, V., Cadule, P., Doney, S.,  
 768 Eby, M., Fung, I., Bala, G., John, J., Jones, C., Joos, F., Kato, T., Kawamiya, M., Knorr, W.,  
 769 Lindsay, K., Matthews, H. D., Raddatz, T., Rayner, P., Reick, C., Roeckner, E., Schnitzler, K.  
 770 G., Schnur, R., Strassmann, K., Weaver, A. J., Yoshikawa, C., and Zeng, N.: Climate–Carbon  
 771 Cycle Feedback Analysis: Results from the C4MIP Model Intercomparison, *Journal of Climate*,  
 772 19, 3337-3353, 2006.  
 773 Fung, I. Y., Doney, S. C., Lindsay, K., and John, J.: Evolution of carbon sinks in a changing  
 774 climate, *Proceedings of the National Academy of Sciences of the United States of America*, 102,  
 775 11201-11206, 2005.  
 776 Galen, C. and Stanton, M. L.: Responses of Snowbed Plant Species to Changes in Growing-  
 777 Season Length, *Ecology*, 76, 1546-1557, 1995.  
 778 Ghimire, B., Riley, W. J., Koven, C. D., Mu, M., and Randerson, J. T.: Representing leaf and  
 779 root physiological traits in CLM improves global carbon and nitrogen cycling predictions,  
 780 *Journal of Advances in Modeling Earth Systems*, 8, 598-613, 2016.  
 781 Govindasamy, B., Thompson, S., Mirin, A., Wickett, M., Caldeira, K., and Delire, C.: Increase  
 782 of carbon cycle feedback with climate sensitivity: results from a coupled climate and carbon  
 783 cycle model, *Tellus B*, 57, 2011.

784 Groendahl, L., Friborg, T., and Soegaard, H.: Temperature and snow-melt controls on  
785 interannual variability in carbon exchange in the high Arctic, *Theoretical and Applied*  
786 *Climatology*, 88, 111-125, 2007.

787 Grogan, P. and Chapin Iii, F. S.: Arctic Soil Respiration: Effects of Climate and Vegetation  
788 Depend on Season, *Ecosystems*, 2, 451-459, 1999.

789 Hartman, M. D., Baron, J. S., Lammers, R. B., Cline, D. W., Band, L. E., Liston, G. E., and  
790 Tague, C.: Simulations of snow distribution and hydrology in a mountain basin, *Water Resources*  
791 *Research*, 35, 1587-1603, 1999.

792 Helfricht, K., Schöber, J., Seiser, B., Fischer, A., Stötter, J., and Kuhn, M.: Snow accumulation  
793 of a high alpine catchment derived from LiDAR measurements, *Adv. Geosci.*, 32, 31-39, 2012.

794 Hinkel, K. M., Eisner, W. R., Bockheim, J. G., Nelson, F. E., Peterson, K. M., and Dai, X.:  
795 Spatial Extent, Age, and Carbon Stocks in Drained Thaw Lake Basins on the Barrow Peninsula,  
796 Alaska, Arctic, Antarctic and Alpine Research, 35, 291-300, 2003.

797 Hinkel, K. M., Frohn, R. C., Nelson, F. E., Eisner, W. R., and Beck, R. A.: Morphometric and  
798 spatial analysis of thaw lakes and drained thaw lake basins in the western Arctic Coastal Plain,  
799 Alaska, *Permafrost and Periglacial Processes*, 16, 327-341, 2005.

300 Hinzman, L. D. and Kane, D. L.: Potential repsonse of an Arctic watershed during a period of  
301 global warming, *Journal of Geophysical Research: Atmospheres*, 97, 2811-2820, 1992.

302 Holland, M. M. and Bitz, C. M.: Polar amplification of climate change in coupled models,  
303 *Climate Dynamics*, 21, 221-232, 2003.

304 Jiang, D., Zhang, Y., and Lang, X.: Vegetation feedback under future global warming,  
305 *Theoretical and Applied Climatology*, 106, 211-227, 2011.

306 Jones, C. D., Cox, P. M., Essery, R. L. H., Roberts, D. L., and Woodage, M. J.: Strong carbon  
307 cycle feedbacks in a climate model with interactive CO<sub>2</sub> and sulphate aerosols, *Geophysical*  
308 *Research Letters*, 30, 1479, 2003.

309 Jones, H. G.: The ecology of snow-covered systems: a brief overview of nutrient cycling and life  
310 in the cold, *Hydrological Processes*, 13, 2135-2147, 1999.

311 Jordan, R. E.: One-dimensional temperature model for a snow cover : technical documentation  
312 for SNTHERM.89, Cold Regions Research and Engineering Laboratory (U.S.) Engineer  
313 Research and Development Center (U.S.), 1991.

314 Jorgenson, M. T., Shur, Y. L., and Pullman, E. R.: Abrupt increase in permafrost degradation in  
 315 Arctic Alaska, *Geophysical Research Letters*, 33, L02503, 2006.  
 316 Koven, C. D., Lawrence, D. M., and Riley, W. J.: Permafrost carbon–climate feedback is  
 317 sensitive to deep soil carbon decomposability but not deep soil nitrogen dynamics, *Proceedings*  
 318 *of the National Academy of Sciences*, 112, 3752-3757, 2015.  
 319 Koven, C. D., Riley, W. J., Subin, Z. M., Tang, J. Y., Torn, M. S., Collins, W. D., Bonan, G. B.,  
 320 Lawrence, D. M., and Swenson, S. C.: The effect of vertically resolved soil biogeochemistry and  
 321 alternate soil C and N models on C dynamics of CLM4, *Biogeosciences*, 10, 7109-7131, 2013.  
 322 Koven, C. D., Ringeval, B., Friedlingstein, P., Ciais, P., Cadule, P., Khvorostyanov, D., Krinner,  
 323 G., and Tarnocai, C.: Permafrost carbon-climate feedbacks accelerate global warming,  
 324 *Proceedings of the National Academy of Sciences*, 108, 14769-14774, 2011.  
 325 Lawrence, D. M. and Swenson, S. C.: Permafrost response to increasing Arctic shrub abundance  
 326 depends on the relative influence of shrubs on local soil cooling versus large-scale climate  
 327 warming, *Environmental Research Letters*, 6, 045504, 2011.  
 328 Liston, G. E. and Elder, K.: A Distributed Snow-Evolution Modeling System (SnowModel),  
 329 *Journal of Hydrometeorology*, 7, 1259-1276, 2006.  
 330 Liston, G. E., Haehnel, R. B., Sturm, M., Hiemstra, C. A., Berezovskaya, S., and Tabler, R. D.:  
 331 Instruments and Methods  
 332 <http://pub2web.metastore.ingenta.com/ns/>  
 332 Simulating complex snow distributions in windy environments using SnowTran-3D, *Journal of*  
 333 *Glaciology*, 53, 241-256, 2007.  
 334 Lopez-Moreno, J. I., Fassnacht, S. R., Begueria, S., and Latron, J.: Variability of snow depth at  
 335 the plot scale: implications for mean depth estimation and sampling strategies, 2011. 2011.  
 336 López-Moreno, J. I., Revuelto, J., Fassnacht, S. R., Azorín-Molina, C., Vicente-Serrano, S. M.,  
 337 Morán-Tejeda, E., and Sexstone, G. A.: Snowpack variability across various spatio-temporal  
 338 resolutions, *Hydrological Processes*, doi: 10.1002/hyp.10245, 2014. n/a-n/a, 2014.  
 339 Luce, C. H., Tarboton, D. G., and Cooley, K. R.: The influence of the spatial distribution of snow  
 340 on basin-averaged snowmelt, *Hydrological Processes*, 12, 1671-1683, 1998.  
 341 Lundquist, J. D. and Dettinger, M. D.: How snowpack heterogeneity affects diurnal streamflow  
 342 timing, *Water Resources Research*, 41, W05007, 2005.



343 Matthews, H. D., Eby, M., Ewen, T., Friedlingstein, P., and Hawkins, B. J.: What determines the  
 344 magnitude of carbon cycle-climate feedbacks?, *Global Biogeochemical Cycles*, 21, [GB2012](#),  
 345 2007a.

346 Matthews, H. D., Eby, M., Ewen, T., Friedlingstein, P., and Hawkins, B. J.: What determines the  
 347 magnitude of carbon cycle-climate feedbacks?, *Global Biogeochemical Cycles*, 21, [n/a-n/a](#),  
 348 2007b.

349 Matthews, H. D., Weaver, A. J., and Meissner, K. J.: Terrestrial Carbon Cycle Dynamics under  
 350 Recent and Future Climate Change, *Journal of Climate*, 18, 1609-1628, 2005.

351 McFadden, J. P., Chapin, F. S., and Hollinger, D. Y.: Subgrid-scale variability in the surface  
 352 energy balance of arctic tundra, *Journal of Geophysical Research: Atmospheres*, 103, 28947-  
 353 28961, 1998.

354 McGuire, A. D., Klein, J. S., Melillo, J. M., Kicklighter, D. W., Meier, R. A., Vorosmarty, C. J.,  
 355 and Serreze, M. C.: Modelling carbon responses of tundra ecosystems to historical and projected  
 356 climate: sensitivity of pan-Arctic carbon storage to temporal and spatial variation in climate,  
 357 *Global Change Biology*, 6, 141-159, 2000.

358 Mefford, T. K., Bieniulis, M., Halter, B., and Peterson, J.: *Meteorological Measurements*, 17 pp.,  
 359 1996.

360 Miller, P. C., Stoner, W. A., and Tieszen, L. L.: A Model of Stand Photosynthesis for the Wet  
 361 Meadow Tundra at Barrow, Alaska, *Ecology*, 57, 411-430, 1976.

362 Montaldo, N. and Albertson, J. D.: Temporal dynamics of soil moisture variability: 2.  
 363 Implications for land surface models, *Water Resources Research*, 39, n/a-n/a, 2003.

364 Morgner, E., Elberling, B., Strebel, D., and Cooper, E. J.: The importance of winter in annual  
 365 ecosystem respiration in the High Arctic: effects of snow depth in two vegetation types, *Polar*  
 366 *Research*, 29, 58-74, 2010.

367 Nobrega, S. and Grogan, P.: Deeper Snow Enhances Winter Respiration from Both Plant-  
 368 associated and Bulk Soil Carbon Pools in Birch Hummock Tundra, *Ecosystems*, 10, 419-431,  
 369 2007.

370 Oberbauer, S. F., Tenhunen, J. D., and Reynolds, J. F.: Environmental Effects on CO<sub>2</sub> Efflux  
 371 from Water Track and Tussock Tundra in Arctic Alaska, U.S.A, *Arctic and Alpine Research*, 23,  
 372 162-169, 1991.

Gautam Bisht 11/14/2017 1:02 PM

Deleted: n/a-n/a

Gautam Bisht 11/14/2017 1:02 PM

Deleted: GB2012

375 Oechel, W. C., Hastings, S. J., Vourltis, G., Jenkins, M., Riechers, G., and Grulke, N.: Recent  
 376 change of Arctic tundra ecosystems from a net carbon dioxide sink to a source, *Nature*, 361, 520-  
 377 523, 1993.

378 Oleson, K. W., D.M. Lawrence, G.B. Bonan, B. Drewniak, M. Huang, C.D. Koven, S. Levis, F.  
 379 Li, W.J. Riley, Z.M. Subin, S.C. Swenson, P.E. Thornton, A. Bozbiyik, R. Fisher, E. Kluzek, J.-  
 380 F. Lamarque, P.J. Lawrence, L.R. Leung, W. Lipscomb, S. Muszala, D.M. Ricciuto, W. Sacks,  
 381 Y. Sun, J. Tang, Z.-L. Yang: Technical Description of version 4.5 of the Community Land  
 382 Model (CLM), National Center for Atmospheric Research, Boulder, CO, [422 pp.](#), 2013a.

383 Oleson, K. W., D.M. Lawrence, G.B. Bonan, B. Drewniak, M. Huang, C.D. Koven, S. Levis, F.  
 384 Li, W.J. Riley, Z.M. Subin, S.C. Swenson, P.E. Thornton, A. Bozbiyik, R. Fisher, E. Kluzek, J.-  
 385 F. Lamarque, P.J. Lawrence, L.R. Leung, W. Lipscomb, S. Muszala, D.M. Ricciuto, W. Sacks,  
 386 Y. Sun, J. Tang, Z.-L. Yang: Technical Description of version 4.5 of the Community Land  
 387 Model (CLM), National Center for Atmospheric Research, Boulder, CO, [2013b](#).

388 Pau, G. S. H., Bisht, G., and Riley, W. J.: A reduced-order modeling approach to represent  
 389 subgrid-scale hydrological dynamics for land-surface simulations: application in a polygonal  
 390 tundra landscape, *Geosci. Model Dev.*, 7, 2091-2105, 2014.

391 Randerson, J. T., Lindsay, K., Munoz, E., Fu, W., Moore, J. K., Hoffman, F. M., Mahowald, N.  
 392 M., and Doney, S. C.: Multicentury changes in ocean and land contributions to the climate-  
 393 carbon feedback, *Global Biogeochemical Cycles*, 29, 744-759, 2015.

394 Rogers, M. C., Sullivan, P. F., and Welker, J. M.: Evidence of Nonlinearity in the Response of  
 395 Net Ecosystem CO<sub>2</sub> Exchange to Increasing Levels of Winter Snow Depth in the High Arctic of  
 396 Northwest Greenland, *Arctic, Antarctic, and Alpine Research*, 43, 95-106, 2011.

397 Rohrbough, J. A., Davis, D. R., and Bales, R. C.: Spatial variability of snow chemistry in an  
 398 alpine snowpack, southern Wyoming, *Water Resources Research*, 39, 1190, 2003.

399 Schaefer, K., Zhang, T., Bruhwiler, L., and Barrett, A. P.: Amount and timing of permafrost  
 900 carbon release in response to climate warming, *Tellus B*, 63, 165-180, 2011.

901 Schimel, J. P., Bilbrough, C., and Welker, J. M.: Increased snow depth affects microbial activity  
 902 and nitrogen mineralization in two Arctic tundra communities, *Soil Biology and Biochemistry*,  
 903 36, 217-227, 2004.

904 Schuur, E. A. G. and Abbott, B.: Climate change: High risk of permafrost thaw, *Nature*, 480, 32-  
 905 33, 2011.

Gautam Bisht 11/14/2017 1:02 PM

Deleted: 422 pp.,

907 Schuur, E. A. G., Bockheim, J., Canadell, J. G., Euskirchen, E., Field, C. B., Goryachkin, S. V.,  
 908 Hagemann, S., Kuhry, P., Lafleur, P. M., Lee, H., Mazhitova, G., Nelson, F. E., Rinke, A.,  
 909 Romanovsky, V. E., Shiklomanov, N., Tarnocai, C., Venevsky, S., Vogel, J. G., and Zimov, S.  
 910 A.: Vulnerability of Permafrost Carbon to Climate Change: Implications for the Global Carbon  
 911 Cycle, *BioScience*, 58, 701-714, 2008.  
 912 Seppala, M., Gray, J., and Ricard, J.: Development of low-centred ice-wedge polygons in the  
 913 northernmost Ungava Peninsular, Québec, Canada, *Boreas*, 20, 259-285, 1991.  
 914 Sexstone, G. A. and Fassnacht, S. R.: What drives basin scale spatial variability of snowpack  
 915 properties in northern Colorado?, *The Cryosphere*, 8, 329-344, 2014.  
 916 Sitch, S., Huntingford, C., Gedney, N., Levy, P. E., Lomas, M., Piao, S. L., Betts, R., Ciais, P.,  
 917 Cox, P., Friedlingstein, P., Jones, C. D., Prentice, I. C., and Woodward, F. I.: Evaluation of the  
 918 terrestrial carbon cycle, future plant geography and climate-carbon cycle feedbacks using five  
 919 Dynamic Global Vegetation Models (DGVMs), *Global Change Biology*, 14, 2015-2039, 2008.  
 920 Smith, L. C., Sheng, Y., MacDonald, G. M., and Hinzman, L. D.: Disappearing Arctic Lakes,  
 921 *Science*, 308, 1429-1429, 2005.  
 922 Smith, M. B., Koren, V., Reed, S., Zhang, Z., Zhang, Y., Moreta, F., Cui, Z., Mizukami, N.,  
 923 Anderson, E. A., and Cosgrove, B. A.: The distributed model intercomparison project – Phase 2:  
 924 Motivation and design of the Oklahoma experiments, *Journal of Hydrology*, 418, 3-16, 2012.  
 925 Smith, N. V., Saatchi, S. S., and Randerson, J. T.: Trends in high northern latitude soil freeze and  
 926 thaw cycles from 1988 to 2002, *Journal of Geophysical Research: Atmospheres*, 109, D12101,  
 927 2004.  
 928 Sturm, M., Douglas, T., Racine, C., and Liston, G. E.: Changing snow and shrub conditions  
 929 affect albedo with global implications, *Journal of Geophysical Research: Biogeosciences*, 110,  
 930 G01004, 2005.  
 931 [Sturm, M., Racine, C., and Tape, K.: Increasing shrub abundance in the Arctic, \*Nature\*, 411, 546,](#)  
 932 [2001.](#)  
 933 Sullivan, P.: Snow distribution, soil temperature and late winter CO<sub>2</sub> efflux from soils near the  
 934 Arctic treeline in northwest Alaska, *Biogeochemistry*, 99, 65-77, 2010.  
 935 Swenson, S. C. and Lawrence, D. M.: A new fractional snow-covered area parameterization for  
 936 the Community Land Model and its effect on the surface energy balance, *Journal of Geophysical*  
 937 *Research: Atmospheres*, 117, n/a-n/a, 2012.

938 Tang, J. and Riley, W. J.: Large uncertainty in ecosystem carbon dynamics resulting from  
 939 ambiguous numerical coupling of carbon and nitrogen biogeochemistry: A demonstration with  
 940 the ACME land model, *Biogeosciences Discuss.*, 2016, 1-27, 2016.

941 [Tape, K. E. N., Sturm, M., and Racine, C.: The evidence for shrub expansion in Northern Alaska](#)  
 942 [and the Pan-Arctic, \*Global Change Biology\*, 12, 686-702, 2006.](#)

943 Tarnocai, C., Canadell, J. G., Schuur, E. A. G., Kuhry, P., Mazhitova, G., and Zimov, S.: Soil  
 944 organic carbon pools in the northern circumpolar permafrost region, *Global Biogeochemical*  
 945 *Cycles*, 23, GB2023, 2009.

946 Thompson, S. L., Govindasamy, B., Mirin, A., Caldeira, K., Delire, C., Milovich, J., Wickett,  
 947 M., and Erickson, D.: Quantifying the effects of CO<sub>2</sub>-fertilized vegetation on future global  
 948 climate and carbon dynamics, *Geophysical Research Letters*, 31, L23211, 2004.

949 Wadham, J. L., Hallam, K. R., Hawkins, J., and O'Connor, A.: Enhancement of snowpack  
 950 inorganic nitrogen by aerosol debris, *Tellus B*, 58, 229-241, 2006.

951 Wahren, C. H. A., Walker, M. D., and Bret-Harte, M. S.: Vegetation responses in Alaskan arctic  
 952 tundra after 8 years of a summer warming and winter snow manipulation experiment, *Global*  
 953 *Change Biology*, 11, 537-552, 2005.

954 Wainwright, H. M., Dafflon, B., Smith, L. J., Hahn, M. S., Curtis, J. B., Wu, Y., Ulrich, C.,  
 955 Peterson, J. E., Torn, M. S., and Hubbard, S. S.: Identifying multiscale zonation and assessing  
 956 the relative importance of polygon geomorphology on carbon fluxes in an Arctic tundra  
 957 ecosystem, *Journal of Geophysical Research: Biogeosciences*, 120, 788-808, 2015.

958 Walker, D. A., Raynolds, M. K., Daniëls, F. J. A., Einarsson, E., Elvebakk, A., Gould, W. A.,  
 959 Katenin, A. E., Kholod, S. S., Markon, C. J., Melnikov, E. S., Moskalenko, N. G., Talbot, S. S.,  
 960 Yurtsev, B. A., and The other members of the, C. T.: The Circumpolar Arctic vegetation map,  
 961 *Journal of Vegetation Science*, 16, 267-282, 2005.

962 Warscher, M., Strasser, U., Kraller, G., Marke, T., Franz, H., and Kunstmann, H.: Performance  
 963 of complex snow cover descriptions in a distributed hydrological model system: A case study for  
 964 the high Alpine terrain of the Berchtesgaden Alps, *Water Resources Research*, 49, 2619-2637,  
 965 2013.

966 Welker, J. M., Fahnestock, J. T., and Jones, M. H.: Annual CO<sub>2</sub> Flux in Dry and Moist Arctic  
 967 Tundra: Field Responses to Increases in Summer Temperatures and Winter Snow Depth,  
 968 *Climatic Change*, 44, 139-150, 2000.

969 Wiggins, I. L.: The distribution of vascular plants on polygonal ground near Point Barrow,  
 970 Alaska, Stanford University Contributions of the Dudley Herbarium, 4, 41-52, 1951.  
 971 Williams, M. W., Hood, E., and Caine, N.: Role of organic nitrogen in the nitrogen cycle of a  
 972 high-elevation catchment, Colorado Front Range, Water Resources Research, 37, 2569-2581,  
 973 2001.  
 974 Williams, T. and Flanagan, L.: Effect of changes in water content on photosynthesis,  
 975 transpiration and discrimination against  $^{13}\text{CO}_2$  and  $\text{C}^{18}\text{O}^{16}\text{O}$  in *Pleurozium* and *Sphagnum*,  
 976 *Oecologia*, 108, 38-46, 1996.  
 977 Wu, Y., Hubbard, S. S., Ulrich, C., and Wulfschleger, S. D.: Remote Monitoring of Freeze–  
 978 Thaw Transitions in Arctic Soils Using the Complex Resistivity Method, *gsvadzone*, 2013. 2013.  
 979 Xu, X., Riley, W. J., Koven, C. D., Billesbach, D. P., Chang, R. Y. W., Commane, R.,  
 980 Euskirchen, E. S., Hartery, S., Harazono, Y., Iwata, H., McDonald, K. C., Miller, C. E., Oechel,  
 981 W. C., Poulter, B., Raz-Yaseef, N., Sweeney, C., Torn, M., Wofsy, S. C., Zhang, Z., and Zona,  
 982 D.: A multi-scale comparison of modeled and observed seasonal methane emissions in northern  
 983 wetlands, *Biogeosciences*, 13, 5043-5056, 2016.  
 984 Zeng, N., Qian, H., Munoz, E., and Iacono, R.: How strong is carbon cycle-climate feedback  
 985 under global warming?, *Geophysical Research Letters*, 31, L20203, 2004.  
 986 Zeng, X. and Decker, M.: Improving the Numerical Solution of Soil Moisture–Based Richards  
 987 Equation for Land Models with a Deep or Shallow Water Table, *Journal of Hydrometeorology*,  
 988 10, 308-319, 2009.  
 989 Zhu, Q., Iversen, C. M., Riley, W. J., Slette, I. J., and Vander Stel, H. M.: Root traits explain  
 990 observed tundra vegetation nitrogen uptake patterns: Implications for trait-based land models,  
 991 *Journal of Geophysical Research: Biogeosciences*, 121, 3101-3112, 2016.  
 992 Zhu, Q. and Riley, W. J.: Improved modelling of soil nitrogen losses, *Nature Clim. Change*, 5,  
 993 705-706, 2015.  
 994 Zona, D., Lipson, D. A., Zulueta, R. C., Oberbauer, S. F., and Oechel, W. C.: Microtopographic  
 995 controls on ecosystem functioning in the Arctic Coastal Plain, *Journal of Geophysical Research:*  
 996 *Biogeosciences*, 116, G00I08, 2011.  
 997